Copyright

by

Joshua Joseph Garvin

2010

The Thesis Committee for Joshua Joseph Garvin
Certifies that this is the approved version of the following thesis

Effect of Anode Properties on the Performance of a Direct Methanol Fuel Cell

APPROVED BY
SUPERVISING COMMITTEE:

Supervisor:

Jeremy Meyers

Carlos Hidrovo

Effect of Anode Properties on the Performance of a Direct Methanol Fuel Cell

by

Joshua Joseph Garvin, BS

Thesis

Presented to the Faculty of the Graduate School of

The University of Texas at Austin

in Partial Fulfillment

of the Requirements

for the Degree of

Master of Science in Engineering

The University of Texas at Austin

December 2010

Acknowledgements

I would like to thank my advisor Dr. Jeremy Meyers for his guidance throughout my Masters program. He was essential in my research by explaining key concepts in fuel cell modeling and helping me formulate the key governing equations for the direct methanol fuel cell modeling. I would also like to thank him for his career advice and making himself available for my numerous questions throughout the research process.

I would also like to thank the Meyers Research Group for their support and encouragement in my coursework and in my research. They were indispensable when I first came to the research group for explaining the eccentricities of modeling and offering me various ways of solving sets of coupled partial differential equations.

I would like to thank other faculty at UT that helped point me in the right direction in terms of vapor liquid equilibrium inside a porous media. Equilibrium in the presence of a capillary pressure difference inside porous media is often not taken into account in many fields and they guided me to resources I could use to model it in my research.

Lastly, I would like to thank my friends and family for their support and encouraging me during my most frustrating times. When I had difficulty obtaining a solution to a problem or my model was giving me unexpected results, they continually assured me that eventually I would figure it out.

August 2010

Abstract

Effect of Anode Properties on the Performance of a Direct Methanol Fuel Cell

Joshua Joseph Garvin, M.S.E.

The University of Texas at Austin, 2010

Supervisor: Jeremy Meyers

This thesis is an investigation of the anode of a direct methanol fuel cell (DMFC) through numerical modeling and simulation. This model attempts to help better understand the two phase flow phenomena in the anode as well as to explain some of the many problems on the anode side of a DMFC and show how changing some of the anode side properties could alleviate these problems. This type of modeling is important for designing and optimizing the DMFC for specific applications like portable electronics. Understanding the losses within the DMFC like removable of carbon dioxide, conversion losses, and methanol crossover from the anode to the cathode will help the DMFC become more commercially viable. The model is based on two phase flow in porous media combined with equilibrium between phases in a porous media with contributions from a capillary pressure difference. The effect of the physical parameters of the fuel cell like the thickness, permeability, and contact angle as well as the operating conditions like the temperature and methanol feed concentration, have on the performance of the DMFC during operation will be investigated. This will show how to remove the gas phase from the anode while enabling methanol to reach the catalyst layer and minimizing methanol crossover.

Table of Contents

Chapter 1: Background 1

1.1 Introduction 1

1.2 Fuel Cell Structure and Operation 2

1.3 Literature Review 3

1.4 Issues in Direct Methanol Fuel Cells 6

1.4.1 Membrane Domain: Methanol and Water Crossover 6

1.4.2 Gas Formation on the Anode Side 7

1.4.3 Other Critical Issues 8

1.5 Mass Transport 8

1.5.1 Two Phase Flow 9

1.5.2 Liquid and Gas Phase Transport: Model 1 11

1.5.3 Liquid Phase Transport: Model 2 12

1.5.4 Gas Phase Transport: Model 2 13

1.6 Vapor-Liquid Equilibrium 15

1.6.1 SRK EOS 17

1.6.2 MHV1 Mixing Rule 18

1.6.3 UNIQUAC 19

1.6.4 Flash Calculation 20

1.6.5 Equilibrium in a Porous Media 21

1.6.6 Bubble Detachment Size 22

1.7 Governing equations 23

1.7.1 Governing Equations: Model 1 23

1.7.2 Governing Equations: Model 2 23

1.8 Numerical Methods 24

1.8.1 Finite-Difference Method 25

1.8.2 Control Volume Approach to Fluxes 26

1.8.3 Newton-Raphson Method 26

Chapter 2: Model Structure....29
2.1 Finite Difference Scheme....29
2.2 Boundary Conditions....30
2.2.1 Model 1....30
2.2.2 Flash Calculation....31
2.2.3 Model 2....31
2.3 Convergence....32
2.4 Material Property Data....33
Chapter 3: Results....34
3.1 Model 1....34
3.1.1 Contact Angle....36
3.1.2 Absolute Permeability....38
3.1.3 GDL Thickness....40
3.2 Flash Calculation....42
3.3 Model 2....45
3.3.1 Contact Angle....49
3.3.2 Absolute Permeability....50
3.3.3 Bubble Detachment Size....52
3.3.4 Limiting Current Density....53
3.3.5 Flux at Boundary....55
3.3.6 Conclusions....56
3.3.7 Other Model Uses....58
Appendix A Material Property Data....60
Appendix B Peng Robinson Equation of State....63
Works Cited....64
Vita....67

Chapter 1: Background

1.1 INTRODUCTION

Direct methanol fuel cells (DMFCs) are ideal for powering portable devices. Unlike batteries, they don't require an existing external power source to be recharged, can be refueled within minutes, and can operate at low temperatures by generating their own waste heat. DMFCs have a much higher specific energy density than the best lithium ion batteries, which means that they can replace batteries in portable electronic devices to significantly increase operation times. Currently, DMFCs are mostly used to power mobile phones, but there is interest in them to supply power to laptops, soldier's equipment, and for charging batteries. One of the main drawbacks of employing DMFCs to replace batteries is their comparatively high costs, which stems from the expensive platinum catalysts and their manufacturing. There are also other important obstacles that need to be addressed before they can be extensively commercialized.

One of the many technical issues in the operation of DMFCs is that of multicomponent mass transport of the reactant and product species. These mass transport problems occur in all of the domains of the fuel cell, including the fuel or gas channels, diffusion layers, catalyst layers, and the membrane. One of the critical domains is the anode diffusion layer whose mass transport issues can negatively affect the transport in the membrane, cathode catalyst layer, and anode fuel channel. Mass transport issues affect the performance of the fuel cell, its stability, and energy density. Only 30% of the chemical energy stored in methanol fuel can be converted into electricity because of losses due to mass transport and heat generation during chemical reactions.

It is necessary to have an understanding of how the physical properties and operating conditions of a DMFC affect its performance. It is also imperative to have a

detailed understanding of the distribution of species inside the anode as well critical mass transport properties like the capillary pressure, saturation, and species flux. All of these pieces are intimately related and must be accounted for when optimizing the DMFC for a specific application.

1.2 Fuel Cell Structure and Operation

A DMFC consists of a membrane-electrode assembly (MEA) in which the electrochemical reactions take place to produce electricity, bipolar plates which serve as the electrical connects, or current collectors, of the fuel cell and provide the fuel through channels. They also consist of gaskets to keep the fuels, both liquid and gas, in their designated regions in the fuel cell.

The MEA is one of the most important parts of a fuel cell. It is composed of gas diffusion layers (GDLs), a polymer electrolyte membrane, an anode, and a cathode. The GDL must be porous and electrically conductive so that methanol (MeOH) can flow from the bipolar plate to anode catalyst layer on one side, and oxygen can flow to the cathode catalyst layer. Most GDL's are composed of carbon of some form, either as a cloth or non-woven fibers.

The polymer electrolyte membrane, also called a separator, serves to conduct protons from the anode to cathode while blocking the passage of electrons. The membrane should also block the passage of MeOH from the anode to cathode, oxidants in the reverse direction, as well as being chemically stable. Most membranes are made of nafion.

The anode is the part of fuel cell where methanol oxidation occurs through the following overall chemical reaction

$$CH_3OH + H_2O \rightarrow 6H^+ + 6e^- + CO_2 \qquad [1.1]$$

There are several complicated elementary steps which give us this overall reaction. The anode is made up of the anode catalyst layer, which is usually composed of platinum and ruthenium. The theoretical voltage of the anode is .02V relative to a hydrogen reference electrode.

The cathode is the part of the fuel cell where oxygen reduction occurs through the following overall chemical reaction

$$\frac{3}{2}O_2 + 6H^+ + 6e^- \rightarrow 3H_2O \qquad [1.2]$$

Similar to the anode reactions, there are several elementary steps producing this reaction. The cathode is made up of the cathode catalyst layer usually composed of pure platinum. The theoretical voltage of the cathode is 1.23V relative to a hydrogen reference electrode. Combining the anode and cathode voltage, the maximum theoretical operating voltage of the DMFC at standard temperature and pressure is 1.21V, however operating voltages around .7V are usually seen. This is because of losses, which will be discussed in section 1.4.

1.3 LITERATURE REVIEW

There have been several attempts to model the anode of a DMFC. One of the first attempts was made by Baxter et al. [1] who developed a model for the porous anode of a liquid fed DMFC. In this study it was assumed that methanol, water, and carbon dioxide were only present in the liquid phase, and therefore there was no two phase flow included. Many other authors have modeled the fuel cell as only having single phase flow in one or two dimensions [2]-[7]. Some authors have modeled all of the parts of fuel cell including the electrodes and the membrane and a few have included the effects the channels have [2]-[4] [7] [8].

One of the first attempts to model the two phase flow in fuel cells was by Scott, Argyropoulos, and Sundmacher [9]. Their model took into the account the effect of a

liquid phase composed of MeOH and water (H_2O) and a counter flowing gas phase composed entirely of carbon dioxide (CO_2). This model took into account the influence of the flow channel on carbon dioxide gas evolution and methanol transport across the anode GDL, electrode, and membrane. CO_2 was modeled as an ideal gas and the effect of the amount of CO_2 occupying the pores on the cell performance was analyzed.

Two of these authors also performed a flow visualization study of CO_2 evolution patterns in the DMFC fuel channel [10]. They found that certain channel patterns have a tendency to form gas slugs and better designs with large exit areas don't for gas slugs at all, even at high current densities. This is because small fast moving bubbles are formed. Further, they found that increasing the liquid flow rate into the channel helps with gas removal.

A few recent models of the liquid feed DMFC have incorporated more of the species in each of the phases [11]-[17]. At steady state, all three species will be present in both the liquid and gas phases. Wang and Wang developed a one-dimensional two-phase model with multicomponent transport [13]. Notably, they assumed the liquid and gas phase are in thermodynamic equilibrium. They assumed that the gas phase is saturated with H_2O and MeOH vapors and used Henry's law type relationships to calculate the vapor pressures. They also assumed the amount of CO_2 in the liquid phase is the liquid saturation concentration. A few later models have performed a similar analysis but instead of assuming all of the species are in thermodynamic equilibrium across the phase boundary, they take into account the effect of non-equilibrium evaporation and condensation between the phases [14] [18]. They assume that there is a finite phase change rate that is proportional to the area of the surface between the phases as well the difference between the concentration and concentration at saturation. They note that

thermodynamic equilibrium is valid in proton exchange fuel cells (PEFCs), especially in the GDL [18].

Experimental studies on the anode gas diffusion layer of the DMFC have been performed to elucidate exactly what properties of the GDL help to facilitate CO_2 gas removal [18]-[21]. They found that higher wettabilities and smaller contact angles improves the DMFC performance and uniform bubbles with smaller size are formed in the gas channel with hydrophilic GDLs, which also increase the performance of the DMFC.

Oliveira et al. explained that all previous models of the DMFC can be classified as analytical, semi-empirical, and mechanistic [22]. According to them, analytical models rely on simplifying assumptions, semi-empirical models combine differential and algebraic equations with empirical correlations to predict the performance of existing cell designs, and mechanistic models incorporate heat, momentum, mass transport, and electrochemical processes. This model can be classified as a combination of semi empirical and mechanistic models.

The model presented in this thesis was developed to accurately describe the relative amounts and distribution of the three species in each phase and their contribution to the performance and operation of a DMFC. The model was developed not only to predict the performance, but to capture the eccentricities of the anode DMFC over a wide range of operation temperatures, pressures, and fuel concentrations that other models may be incapable of producing. This will not only elucidate what is needed for CO_2 removal from the anode, but also what other losses occur in DMFC operation, and what is needed to improve performance.

1.4 ISSUES IN DIRECT METHANOL FUEL CELLS

1.4.1 Membrane Domain: Methanol and Water Crossover

A significant problem in DMFC operation that leads to poor performance is methanol crossover from the anode catalyst to the cathode catalyst layer.

As stated in Section 1.2, one of the roles of the polymer electrolyte membrane is to prevent the fuels from crossing to the other electrode. Nafion is the most popular polymer electrolyte membrane because of its chemical stability and its good proton conductivity. However, the use of Nafion leads to poor performance of the fuel cell because methanol diffuses through it due to the concentration gradient between the anode and cathode [23]. Methanol's hydroxyl group also interacts with the protons and is dragged to the cathode. Once at the cathode, methanol can be oxidized by oxygen, causing a mixed potential, which lowers the cell voltage. An additional result of this is that the efficiency of the cell is lowered because methanol fuel is wasted.

A solution to this is to use dilute methanol fuel concentrations so less methanol has the potential to crossover, but this is only effective at low currents. At high currents, methanol is consumed quickly and therefore portions of the anode catalyst layer become starved and cell voltage is lowered [23].

Nafion membranes are also permeable to H_2O. Since the concentration of H_2O in the fuel is high, a large portion of H_2O has the capability to flow through the membrane to the cathode. Once at the cathode, it can increase the problem of cathode flooding. In addition to this, if enough H_2O transports through the membrane, additional H_2O needs to be supplied to the anode through a separate system, increasing the complexities of the overall system [23].

Modifications of the nafion membrane and membrane replacements are actively being pursued to alleviate some of these problems [24].

1.4.2 Gas Formation on the Anode Side

Another issue in DMFC operation deals with the two-phase transport on the anode side of the fuel cell. There is a counter flux of MeOH and H_2O flowing to the catalyst layer and carbon dioxide (at low temperatures) flowing to the gas channel to be removed. CO_2 in the gas phase is formed in the anode catalyst layer and through convection and diffusion, flows to the top of gas diffusion layer and out of the GDL to the gas channel. The effect of gas counterflow is twofold. The first effect, which has been studied extensively through visualization and modeling, is that the gas can form large bubbles and slugs in the anode gas channels, which, depending on the operating conditions, can severely hinder methanol from transporting to the catalyst layer [10] [19]. At high current densities, the amount of gas in the channels increases significantly and in certain designs of the gas channels, may even block the entire channel.

A solution to this problem is using GDL's with less surface tension, a broad pore size distribution, and high hydrophilicity [19]. These properties cause small uniform sized bubbles to be produced and results in a regular periodic removal of the bubbles from the back of GDL. The smaller bubbles can be harder to detach from the GDL, however.

The second effect of the two phase flow is that gas bubbles may block a large portion of the pores inside the GDL as well as on the surface. This reduces the transport area for methanol to flow to the catalyst layer. In addition, because the gas flows to the top of GDL, the methanol may not be evenly distributed over the entire electrode [23]. In-plane transport of methanol would be needed to distribute it evenly over the electrode surface.

1.4.3 Other Critical Issues

During methanol oxidation on the anode catalyst layer, several adsorbed species are formed and are not easily oxidized to other species. Therefore they remain adsorbed on catalyst layer and block methanol from reaching those catalytic sites. The oxidation of these intermediates is the rate limiting step in methanol oxidation. Related to this is the degradation of the DMFC cathode catalyst layer. The catalyst layer decays due to the growth and poisoning of the catalyst. During operation, Ruthenium crosses over through the membrane from the anode and deposits on the cathode, limiting oxygen reduction and thus degrading the overall cell performance [24].

Another loss of performance in the DMFC comes from excess heat generation. The oxidation of methanol at the cathode after it crosses over produces heat. This heat causes the membrane to swell increasing the methanol crossover [24]. It also increases the H_2O pressure in the cathode, limiting the reduction of hydrogen because of a lack of oxygen.

1.5 MASS TRANSPORT

In this study, before the complete two phase equilibrium model was developed, a simpler two-phase model was constructed. In this simpler model, two phase flow was modeled, but the liquid phase was composed of only MeOH and H_2O, and the gas phase, CO_2. Therefore, equilibrium between the species in different phases was not included. In the following formulation of the equations of mass transport, the sets of equations for both models will be described. The simpler model will be referred to as model 1 and the full model with equilibrium will be referred to as model 2.

1.5.1 Two Phase Flow

Inside the anode GDL of a DMFC, there is two phase flow at the operating methanol concentrations and temperatures of interest. A diagram of this two phase flow is shown in Figure 1.

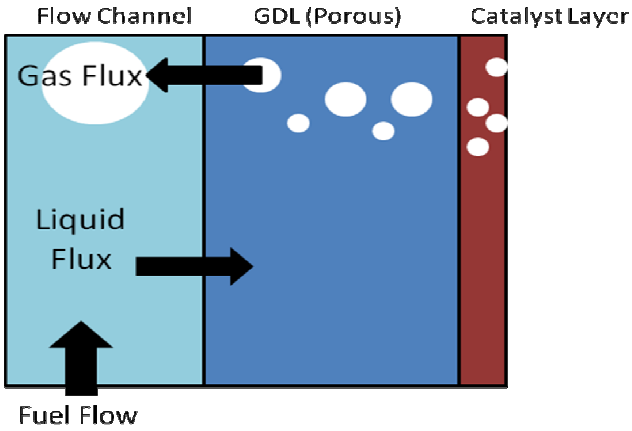

Figure 1: Diagram of the anode side of a fuel cell with two phase counter flow

In Figure 1, the gas and liquid fluxes are the convective fluxes. The arrows indicate the direction in which the driving force in convection, the gradient in pressure, is forcing the gas and liquid. The gas is produced in the catalyst layer and must flow from the catalyst layer through the GDL and out of the cell through the flow, or fuel channel. There is a counter flux of liquid from the fuel channel to the catalyst layer. In model 1, the gas flux is entirely that of CO_2, while in model 2, the gas flux is the flux of all three species. Similarly, in model 1 the liquid flux is that of liquid MeOH and H_2O while in model 2, it is that of all three species.

Within a pore, there is a meniscus and a radius of curvature of the liquid because there is a nonzero capillary pressure inside the pore. The capillary pressure is defined as

$$P_c = P^l - P^v \qquad [1.3]$$

The liquid and gas are in mechanical equilibrium inside the pore. The requirement for mechanical equilibrium inside a pore over a curved interface is that the

difference in pressure between the gas and liquid phases must be equal to the normal stress imposed by the surface tension of the liquid. This equilibrium condition, rearranged to show the critical radius of the pore, is shown in the following expression

$$r_{c,h} = -\frac{2\gamma \cos\theta_{c,h}}{P_c} \quad [1.4]$$

To calculate how much of the pore is filled with liquid H_2O, a liquid saturation is defined as [25] [26],

$$S_h = \sum_k \frac{f_{r,k}}{2}\left[1 + \vartheta_h erf\left(\frac{\ln r_{c,h} - ln\, r_{o,k}}{s_k\sqrt{2}}\right)\right] \quad [1.5]$$

where $f_{r,k}$ is the fraction of the total distribution made up of k, ϑ_h is 1 for hydrophilic pores and -1 for hydrophilic ones, $r_{o,k}$ is the characteristic pore size for the GDL, which depends on the material, and s_k is the spread of distribution k.

Another important parameter for modeling the mass transports inside the GDL is the permeability. The permeability is a measure of how easily a porous material can transport a liquid or solid through its pores. In this study, an effective permeability is used and is defined as

$$k = k_r k_{sat} \quad [1.6]$$

where k_r is the relative liquid or gas permeability and k_{sat} is the absolute permeability of the material, which is a property of the medium and can be found in the literature. k_r for the liquid and gas phases are defined as follows [25] [26]:

$$k_{r|L} = \frac{S_e^{\,2}}{2}\sum_k f_{r,k}\left[1 + \vartheta_h erf\left(\frac{\ln r_{c,h} - lnr_{o,k}}{s_k\sqrt{2}} - s_k\sqrt{2}\right)\right] \quad [1.7]$$

$$k_{r|G} = \left(\frac{1 - S_e}{2}\right)^2\sum_k f_{r,k}\left[1 - \vartheta_h erf\left(\frac{\ln r_{c,h} - lnr_{o,k}}{s_k\sqrt{2}} - s_k\sqrt{2}\right)\right] \quad [1.8]$$

In equations 1.7 and 1.8, S_e is the effective saturation. Instead of using the effective saturation, the saturation in equation 1.5 is used. The effective saturation in equations 1.7 and 1.8, taken from [25], comes from the fact that the saturation never reaches unity because of a residual gas saturation.

1.5.2 Liquid and Gas Phase Transport: Model 1

In model 1, the MeOH is transported by diffusion and convection, and the H_2O is transported by convection only. For MeOH, the molar flux density, or superficial flux, is calculated as follows:

$$N_{MeOH} = -D_{i,j}^{eff} \nabla C_{MeOH} + C_{MeOH} V^l \quad [1.9]$$

$$D_{i,j}^{eff} = (\epsilon_o S_l)^{1.5} D_{i,j} \quad [1.10]$$

$$V^l = -\frac{k}{\mu} \nabla P^l \quad [1.11]$$

$D_{i,j}^{eff}$ is the effective diffusion coefficient which depends on the tortuosity of the medium, ϵ_o is the bulk porosity, $D_{i,j}$ is the binary diffusion coefficient between the MeOH and H_2O in the liquid phase, and C_{MeOH} is the concentration of methanol, V is the velocity of the liquid inside the porous medium, and μ is the viscosity of the mixture which is assumed to be that of H_2O. The exponent of 1.5 in equation 1.10 is taken from the Bruggeman correction, which accounts for both the reduction in cross-sectional area and tortuosity with reduced volume fraction. Though it is an approximation, it is widely used and generally useful for correlation of results. Equation 1.11 is Darcy's law and it is used because there is an expected pressure gradient in the liquid phase. It states that the velocity of the fluid moves in the opposite direction to its pressure gradient. The first

term in equation 1.9 is the diffusion flux and the second term is the convective flux of MeOH.

The flux of H_2O and CO_2 are calculated as follows:

$$N_{H_2O} = C_{H_2O} V^l \quad [1.12]$$

$$N_{CO_2} = C_{CO_2} V^g \quad [1.13]$$

$$C_{CO_2} = \frac{p^v}{RT}$$

$$V^g = -\frac{k}{\mu} \nabla p^g$$

Equation 1.12 means that H_2O is transported by convection only. This is assumed because the most of the fuel is composed of H_2O therefore any diffusion flux of H_2O is negligible. Equation 1.13 means that CO_2 is transported by convection only. It is assumed that the CO_2 can be modeled as an ideal gas, which is shown in the second part of equation 1.13. To calculate its velocity, Darcy's law is also used, however the viscosity is that of CO_2 gas and the pressure is that of the gas phase.

1.5.3 Liquid Phase Transport: Model 2

The liquid mixture is transported by diffusion and convection inside the porous GDL. For the liquid phase, the Fick's diffusion law is used again which is as follows:

$$N = -D_{i,j}^{eff} \frac{1}{V_i} \nabla x_i \quad [1.14]$$

x_i is the liquid phase mole fraction, $D_{i,j}^{eff}$ is calculated from equation 1.10, and $D_{i,j}$ is the binary diffusion coefficient between the species, i, and H_2O, j, in the liquid phase. V_i is the molar volume of the mixture which is approximated as that of H_2O. Because the

majority of the liquid mixture is H_2O, the diffusion of H_2O is not included although there will be some diffusion of liquid H_2O. The exclusion of the diffusion of liquid H_2O should not significantly affect the results of the model.

For convection inside the porous GDL, the classical convection law is used which is as follows:

$$N = \frac{1}{V_i} x_i V^l \qquad [1.15]$$

The velocity of the liquid inside the porous medium is calculated using Darcy's law, equation 1.11.

1.5.4 Gas Phase Transport: Model 2

Every gas species is transported by diffusion and convection. With respect to diffusion, the Stefan-Maxwell equation is used. The Stefan-Maxwell equation describes the diffusion of a gas composed of a multiple number of species. It takes into account the binary interactions between the species, as well as the differences in the velocities. The Stefan-Maxwell equation is defined as follows

$$\mathbf{P}\nabla y_i = \frac{RT}{P^v} \sum_{j \neq i}^{n} \frac{N_j P_i - N_i P_j}{D_{i,j}^{eff}} \qquad [1.16]$$

$$D_{i,j}^{eff} = (\epsilon_\omega (1 - S_h))^{1.5} D_{i,j} \qquad [1.17]$$

where P_i and P_j are the partial pressures of the species, defined in equation 1.18, $D_{i,j}^{eff}$ is the effective binary diffusion coefficient of the gas phase between species i and j, and $D_{i,j}$, is the binary diffusion coefficient between species i and j in the gas phase. Only two of the equations in the Stefan-Maxwell formulation are linearly independent as written in equation 1.16.

Convection in the gas phase is calculated using Darcy's law and by using the mass average velocities. The velocity of the gas phase can be calculated as follows

$$\boldsymbol{V^v} = \frac{\sum_{i \neq j} M_i c_i V^v{}_i}{\sum_{i \neq j} M_i c_i} = RT \frac{\sum_{i \neq j} M_i N_i}{\sum_{i \neq j} M_i P_i} = -\frac{k}{\mu} \nabla P^v \qquad [1.18]$$

$$c_i = y_i \frac{1}{V_i} = \frac{P_i}{RT} = \frac{y_i P^v}{RT}$$

M_i is the molecular mass of the species, c_i is the concentration of the species, and y_i is the mole fraction of the species in the gas phase. The concentration is equal to the mole fraction multiplied by the inverse of the molar volume of the gas mixture which is also equal to the species partial pressure divided by RT. The species are modeled as ideal gasses as shown in the second portion of equation 1.18. To add convection to the Stefan-Maxwell equations, it is necessary to replace one of the equations in 1.16 with equation 1.18. All three fluxes are solved simultaneously f by the following matrix inversion and multiplication:

$$\begin{bmatrix} -\left(\frac{y_2}{D_{12}} + \frac{y_3}{D_{13}}\right) & \frac{y_1}{D_{12}} & \frac{y_1}{D_{13}} \\ \frac{y_3}{D_{13}} & \frac{y_3}{D_{23}} & -\left(\frac{y_2}{D_{23}} + \frac{y_1}{D_{13}}\right) \\ \frac{M_1 RT}{\sum_i^n M_i P_i} & \frac{M_2 RT}{\sum_i^n M_i P_i} & \frac{M_3 RT}{\sum_i^n M_i P_i} \end{bmatrix}^{-1} * \begin{bmatrix} P\nabla y_1 \\ P\nabla y_3 \\ -\frac{k}{\mu} \nabla P^v \end{bmatrix} = \begin{bmatrix} N_1 \\ N_2 \\ N_3 \end{bmatrix} \qquad [1.19]$$

where 1 is CO_2, 2 is H_2O, and 3 is MeOH. Note that diffusion and convection are occur in parallel and therefore are usually additive as shown in the following expression

$$N_i = N^V{}_i + N^D{}_i \qquad [1.20]$$

where the V and D stand for convection and diffusion, respectively. In this model, they are not additive but they are still coupled as seen in equation 1.19.

1.6 VAPOR-LIQUID EQUILIBRIUM

In the DMFC, it is assumed that vapor will be produced as soon as current is drawn from the cell. This is because in most DMFC applications, the fuel is recycled. Once the fuel cell starts producing electricity, the carbon dioxide which is produced in the catalyst layer enters the liquid phase and after a while it becomes saturated with carbon dioxide. Any subsequent carbon dioxide which is produced enters the gas phase. There will also be small mole fractions of MeOH and H_2O in the vapor phase at low temperatures (30 °C) and significant mole fractions at high operation temperatures (90 °C). The result of this is that there will be three species present in both the liquid and vapor phases at all times.

Because the length scales are small, on the order of 10's of μm, it can be assumed that all the species in each phase are well mixed. Further, this means that equilibrium takes place at extremely short time scales [18]. Therefore it is assumed the species in the vapor and liquid phases are in local equilibrium.

From thermodynamics, it is known that at equilibrium between two phases, the temperature, pressure, and partial molar Gibbs free energy must be the same for a species in each phase. Further, the Gibbs free energy is at its minimum value. The partial molar Gibbs free energy is called the chemical potential.

$$\left.\frac{\partial G}{\partial n_i}\right|_{T,P,n_j} = \mu_i \qquad [1.22]$$

Therefore we can assume that the chemical potential of any species in the two phases must be equal.

$$\mu_i^l = \mu_i^v \qquad [1.23]$$

Equivalently, the fugacity of any species in the two phases must also be equal [29].

$$f_i^l = f_i^v \quad [1.24]$$

The fugacity is related to the chemical potential through

$$d\mu = RTdlnf \quad [1.25]$$

There are two ways to solve equation 1.24. The first, which is not used in this study, is called the gamma-phi approach [29]. This approach is suitable for calculations at low pressures, which includes this study. This approach is calculated as follows

$$y_i\varphi_i^v P = x_i\gamma_i P_i^s\varphi_i^s \quad [1.24]$$

γ_i is the activity coefficient of the species in the liquid phase, P_i^s is the saturation or vapor pressure of species, and φ_i^v and φ_i^s are the vapor phase fugacity coefficient and the fugacity coefficient at saturation, respectively. The fugacity and fugacity coefficient are related by

$$\varphi_i = \frac{f_i}{z_i P} \quad [1.26]$$

where z_i is a general mole fraction in either phase. The activity coefficient is usually calculated using a correlative model such as UNIQUAC which will be explained in Section 1.7.

The second method, called the Equation of State (EOS) method or phi-phi method, is as follows [29] –[33]

$$x_i\varphi_i^l = y_i\varphi_i^v \quad [1.27]$$

The fugacity coefficients in each phase are dependent on temperature, pressure, and the composition of the phase. The EOS method was used because the liquid mixture of MeOH and H_2O is non ideal because methanol and H_2O are highly polar substance so a method to take into account their interactions was needed.

1.6.1 SRK EOS

To calculate the fugacity coefficients in each phase for all of the species, the Soave-Redlich-Kwong (SRK) EOS was used. An EOS is a relation between pressure, volume, and temperature and this particular EOS is cubic with respect to volume. The SRK EOS formulation is as follows

$$P = \frac{RT}{(V-b)} - \frac{a}{V(V+b)} \qquad [1.28]$$

$$b = \sum_i z_i b_i$$

$$b_i = .08664\frac{RT_c}{P_c}$$

The T_c and P_c are the critical temperature and pressures of the species. In equation 1.28, the a is the attraction parameter and is dependent on temperature and the shape of the molecules through an acentric factor, and the b is the repulsion parameter and represents the volume of the molecules [30]. Both of these parameters are derived from the critical properties of the species, as well as their relative compositions. This equation of state can be applied to both liquid and vapor species to find several properties including the compressibilies and molar volumes of the liquid and vapor mixtures as well as the fugacity coefficients of all the species in both phases. Because equation 1.21 is cubic with respect to volume, there are three real roots of the molar volume and compressibility factor at the temperatures and pressures of interest. These three real roots are found through the following expressions [31]

$$Z^3 - Z^2 + (A - B - B^2)Z - AB = 0 \qquad [1.29]$$

$$A = \frac{aP}{R^2T^2}$$

$$B = \frac{bP}{RT}$$

$$V = \frac{ZRT}{P}$$

The largest root of equation 1.29 is the vapor compressibility factor while the smallest is the liquid compressibility factor. These are found using the built in functions of min and max in Matlab. The middle root has no physical significance. In order to find the a parameter in equations 1.28 and 1.29, a mixing rule called the Modified Huron Vidal (MHV1) mixing rule is used.

1.6.2 MHV1 Mixing Rule

The MHV1 mixing rule was developed to calculate the a parameter in the SRK EOS (equation 1.28) by incorporating the excess Gibbs free energy at all temperatures and pressures [34]. It is assumed that the a parameter is independent of volume. The derived expression for the MHV1 mixing rule is

$$a = bRT\left(\sum z_i\left(\frac{a_i}{b_i RT}\right) + \frac{1}{q_1}\left[\frac{G_0^E}{RT} + \sum z_i \ln\frac{b}{b_i}\right]\right) \qquad [1.30]$$

$$a_i = 0.42748\frac{R^2 T_c^{\,2}}{P_c}\left(1 + m\left(1 - \sqrt{\frac{T}{T_c}}\right)\right)^2$$

$$m = 0.48 + 1.574\omega - 0.176\omega^2$$

In equation 1.30, ω is the species acentric factor, G_0^E is the excess Gibbs free energy which is predicted by the UNIQUAC model in the following section, and q_1 is a parameter equal to -.593 for the MHV1 mixing rule [34]. The fugacity coefficient of each species in each phase can then be predicted from the following equation

$$\ln\varphi_i = \ln\left(\frac{1}{Z-B}\right) + \left[\frac{\frac{P}{RT}}{Z-B} - \frac{\frac{P\alpha}{RT}}{Z+B}\right]b_i - \left(\frac{1}{q_1}\left(\ln\gamma_i + \ln\frac{b}{b_i} + \frac{b_i}{b} - 1\right) + \alpha_i\right)\ln\left(\frac{Z+B}{Z}\right) \qquad [1.31]$$

$$\alpha = \frac{b}{RT}$$

$$\alpha_i = \frac{b_i}{RT}$$

1.6.3 UNIQUAC

To predict the activity coefficients of all the species in both phases, a Universal Quasichemical (UNIQUAC) model was utilized. UNIQUAC is a lattice model which predicts the activity coefficients based on the physical properties of the species as well as the interaction of the molecules [35]. It is capable of predicting the effect of polar and nonpolar interactions among the species. The model has a combinatorial part which is based on the size and shape of the molecules as well as a residual part which takes into account the intermolecular forces [35]. The UNIQUAC formulation is as follows

$$ln\gamma_i = ln\gamma_i^c + ln\gamma_i^R \qquad [1.32]$$

$$ln\gamma_i^c = ln\frac{\vartheta_i}{z_i} + \frac{Z}{2}q_i ln\frac{\theta_i}{\vartheta_i} + l_i - \frac{\vartheta_i}{z_i}\sum_{j=1}^{c} x_j l_j$$

$$l_j = \frac{Z}{2}(r_j - q_j) - (r_j - 1)$$

$$ln\gamma_i^R = q_i\left[1 - \ln\left(\sum_{j=1}^{c}\theta_j\tau_{ji}\right) - \sum_{j=1}^{c}\left(\frac{\theta_j\tau_{ji}}{\sum_{k=1}^{c}\theta_j\tau_{kj}}\right)\right]$$

$$\vartheta_i = \frac{x_i r_i}{\sum_{i=1}^{c} x_i r_i}$$

$$\theta_i = \frac{x_i q_i}{\sum_{i=1}^{c} x_i q_i}$$

$$r_i = \frac{V_{wi}}{(1.517 * 10^{-2})}$$

$$q_i = \frac{A_{wi}}{(2.5 * 10^{8})}$$

$$\tau_{ji} = e^{-\frac{\Delta u_{ij}}{RT}}$$

$$\frac{G_0^E}{RT} = \sum z_i \, ln \, ln\gamma_i \qquad [1.33]$$

where $ln\gamma_i^C$ is the combinatorial contribution of the activity coefficient, $ln\gamma_i^R$ is the residual contribution of the activity coefficient, Δu_{ij} is the interaction parameter between two species j and I, q_i is the area parameter of species I, r_i is the size parameter of species I, V_{wi} is the van der waals volume (m^3/kmol), A_{wi} is the van der waals area (m^2/kmol), and Z is the coordination number which is set equal to 10 [30]. Because there are 3 species in the fuel, there will be six binary interaction parameters which are defined in Appendix A. The activity coefficients and relative mole fractions are very sensitive to the values of the interaction parameters, therefore a set was chosen which was predicted under concentration, temperature, and pressure conditions close to the ones in this study [36]. Also, the van der waals volumes and areas are tabulated for various molecules [37].

1.6.4 Flash Calculation

In order to find the equilibrium mole fractions at the anode GDL and flow channel interface, a flash calculation must be performed. A flash calculation, also called a flash evaporation, is the vapor that occurs after a saturated liquid passes through a throttle and undergoes a pressure reduction. Note that a flash calculation can only been performed if there are two phases present. To solve a multiphase multicomponent flash calculation, the Rachford-Rice equation must be solved [31] [32] [33]. The Rachford-Rice equation is

$$\sum_i \frac{z_i(K_i - 1)}{1 + \beta(K_i - 1)} = 0 \qquad [1.34]$$

where β is the fraction of the saturated liquid that is vaporized and K_i is the equilibrium constant of species i. The equilibrium constants are also related to the mole fractions and the species fugacities through the following expressions

$$y_i = K_i x_i \qquad [1.35]$$

$$K_i = \frac{\varphi_i^l}{\varphi_i^v} \quad [1.36]$$

The liquid phase mole fractions can be found once the vaporization factor is found from the Rachford-Rice equation through the following equations

$$x_i = \frac{z_i}{1 + \beta(K_i - 1)} \quad [1.37]$$

The correct β is the value which ensures that the liquid and vapor mole fractions are real and positive and also that there are K_i values that are less than 1 and greater than 1.

1.6.5 Equilibrium in a Porous Media

When a fuel cells runs at moderate to high currents, a significant capillary pressure gradient is formed inside the pores of the anode GDL and catalyst layer, enabling the vapor to escape and the liquid to reach the catalyst layers. In most applications of vapor-liquid equilibrium, the pressure of the phases are approximated as equal because the magnitude of the capillary pressure is small compared to the operating pressures. However in certain DMFC applications, significant capillary pressures can form inside the pores relative to the operating pressures. Therefore, it was deemed important to include the capillary effects inside the porous media.

Inside a liquid and vapor filled pore at equilibrium, the pressure inside the gas phase must balance the pressure of the contacting liquid phase. Further for a system at constant temperature, volume, and number of moles, the chemical potential of each species in both phases must be equal as stated in equation 1.22. Therefore, there must be local mechanical and chemical equilibrium [38] [39]. However, the chemical potential of each phase is calculated at its own pressure [38] [39]. For capillary equilibrium, there is an additional degree of freedom when compared to normal equilibrium and this comes in

the form of the two phase pressures. The modification to the previous equilibrium equations (equations 1.22, 1.23 and 1.27) are

$$\mu_i^l(T, P^l, x_i) = \mu_i^v(T, P^v, y_i) \quad [1.38]$$

$$f_i^l(T, P^l, x_i) = f_i^v(T, P^v, y_i) \quad [1.39]$$

$$x_i \varphi_i^l P^l = y_i \varphi_i^v P^v \quad [1.40]$$

In equation 1.40, the fugacity in the liquid and gas phases has to be calculated using the liquid and gas phase pressures, respectively. Further, when performing a flash calculation, the equilibrium constants have to be modified by the inclusion of the pressures as shown in the following equation

$$K_i = \frac{\varphi_i^l P^l}{\varphi_i^v P^v} \quad [1.41]$$

1.6.6 Bubble Detachment Size

An important part of DMFC operation is the removal of the gas phase through the fuel channel. The gas phase flows from the catalyst layer to the fuel channel through the GDL. At the interface of the fuel channel and GDL, the gas, in the form of bubbles, diffuses to the top of the GDL and attach to the backing of the GDL. Once a sufficient amount of bubbles form, they are swept away by the liquid fuel flowing in the fuel channel. The bubble detachment process is dictated by buoyancy and surface tension effects [19]. The diameter of the bubbles at detachment is given by [19]:

$$d_b = \left(\frac{4 d_p \gamma \sin\theta}{g(\rho_l - \rho_g)} \right)^{1/3} \quad [1.42]$$

where d_b is the pore backing size, which can be calculated from the characteristic radius, g is the gravity, and ρ_l and ρ_g are the liquid and gas phase densities, respectively. The gas phase density is calculated the denominator of equation 1.18. It has been found

that small homogenously spread bubbles are easily removed the backing of the GDL and larger ones can coalesce and form slugs inside the fuel channel. In some cases, viscous shear will dominate over buoyancy and will control the detachment process, necessitating a high linear velocity in the anode fuel channels.

1.7 GOVERNING EQUATIONS

1.7.1 Governing Equations: Model 1

In solving a typical multiphase, multicomponent, fluid flow problem, conservation of mass, species, and momentum must be taken into account [40]. In the GDL, conservation of momentum is given by Darcy's law for the liquid and gas phases. Conservation of mass and species are given in the following equations:

$$\nabla N_{CO_2} = 0 = \frac{1}{RT} V^v \nabla P_{CO_2} + \frac{P_{CO_2}}{RT} \nabla V^v \quad [1.43]$$

$$\nabla N_{H_2O} = 0 = C_{H_2O} \nabla V^l \quad [1.44]$$

$$\nabla N_{MeOH} = 0 = -\nabla D^{eff} \nabla C_{MeOH} - D^{eff} \nabla^2 C_{MeOH} + C_{MeOH} \cdot \nabla V^l + V^l \nabla C_{MeOH} \quad [1.45]$$

Because there are chemical reactions taking place inside of the GDL, no species are created or destroyed and therefore the divergence of the flux must be equal to zero (equations 1.43, 1.44, and 1.45). The flux equations which were used are equations 1.9, 1.12, and 1.13. The three variables to be solved are P_{CO_2}, which is the gas pressure P^v, C_{MeOH}, and P^l. The solution method will be discussed in section 1.8.

1.7.2 Governing Equations: Model 2

Similarly, multiphase multicomponent flow in the porous GDL is governed by conservation of mass, species, and momentum. Additionally, relations are needed for the equilibrium of species in the liquid and gas phases. Again, conservation of momentum is

given by Darcy's law in the liquid and gas phases. Conservation of mass, species, and equilibrium are given by the following expressions:

$$\nabla \cdot N^{g}_{H_2O} + \nabla \cdot N^{l}_{H_2O} = 0 \quad [1.46]$$

$$\nabla \cdot N^{g}_{CO_2} + \nabla \cdot N^{l}_{CO_2} = 0 \quad [1.47]$$

$$\nabla \cdot N^{g}_{MeOH} + \nabla \cdot N^{l}_{MeOH} = 0 \quad [1.48]$$

$$x_{CO_2} \varphi^{l}_{CO_2} P^{l} = y_{CO_2} \varphi^{v}_{CO_2} P^{v} \quad [1.49]$$

$$x_{H_2O} \varphi^{l}_{H_2O} P^{l} = y_{H_2O} \varphi^{v}_{H_2O} P^{v} \quad [1.50]$$

$$x_{MeOH} \varphi^{l}_{MeOH} P^{l} = y_{MeOH} \varphi^{v}_{MeOH} P^{v} \quad [1.51]$$

Because there are no chemical reactions taking place, no species can be created or destroyed. However, they can change phase between the gas and liquid phases but the total mass of the species will always be conserved within a control volume.

The conservation of species is given by equations 1.46, 1.47, 1.48. The six variables to be solved for are P^l, P^v, x_{MeOH}, y_{MeOH}, x_{CO_2} and y_{CO_2}. Since the number of moles are conserved because no chemical reactions are occurring, through equations 1.46, 1.47, and 1.48, mass conservation is also satisfied.

1.8 NUMERICAL METHODS

The three and six governing nonlinear partial differential equations for models 1 and 2, respectively, were solved using numerical methods. The GDL was discretized in one dimension into a prescribed number of cells and each cell is bounded by two meshpoints. Each of the six main variables is defined at each meshpoint and other dependent variables like the diffusion coefficients, velocities, and fugacities were also defined at each mesh point. The differential equations were numerically approximated using finite-difference techniques and numerical methods were used to simultaneously solve the equations and determine the correct values of the variables at each mesh point.

1.8.1 Finite-Difference Method

The finite difference method was used to change the analytical derivates and partial differential equations into numerical approximations. In this technique, which is derived from a Taylor series expansion of a function, the derivates are transformed into quotients [41]. Two forms of the finite difference approximation were used which are the forward difference and backward difference forms. In the forward difference form, the derivates are approximated as follows [41]:

$$\left.\frac{dc_i}{dx}\right|_{j+1/2} = \frac{c(j+1) - c(j)}{h} + O(h^2) \qquad [1.52]$$

and the backward difference form is define as follows:

$$\left.\frac{dc_i}{dx}\right|_{j-1/2} = \frac{c(j) - c(j-1)}{h} + O(h^2) \qquad [1.53]$$

In the previous two equations, h is the distance between each mesh point which depends on the number of cells the user provides in the model. With each finite difference approximation, there is an error associated with it, O, which is of the order h^2, that can be reduced by increasing the number of cells or meshpoints in the model. The ½ corresponds to the variable c being defined at half meshpoints, which was done to make the size of the error as small as possible. In this study, the fluxes of each species were defined at half meshpoints. The consequence of this is that other variables in the flux equations must be defined at half meshpoints as well, like the diffusion coefficients:

$$D_i|_{j+1/2} = \frac{D_i(j) + D_i(j+1)}{2} \qquad [1.54]$$

1.8.2 Control Volume Approach to Fluxes

To solve equations 1.43-1.51, a control volume approach was used. A visual example of this is shown in figure 2.

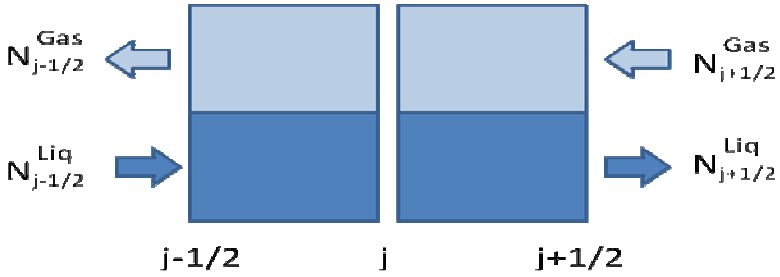

Figure 2: Diagram of the control volume approach to solving for the divergence of the flux in equations 1.46, 1.47, and 1.48.

In the GDL, since there are no chemical reactions occurring and the fuel cell is being run at steady state, the sum of the liquid and gas fluxes at the left of the control volume has to equal the sum at the right of the control volume in Figure 2

$$N^{Gas}{}_{j-1/2} + N^{Liq}{}_{j-1/2} = N^{Gas}{}_{j+1/2} + N^{Liq}{}_{j+1/2} \quad [1.55]$$

1.8.3 Newton-Raphson Method

The Newton-Raphson method, also known as Newton's method, was used to perform the flash calculation and to solve the governing partial differential equations. It is used because it yields quadratic convergence of the equations [41]. In this method, we wish to find the solution of a set of equations of the form

$$g(c) = 0 \quad [1.56]$$

The number of equations, g, must equal of the number of unknowns, c, and it is possible that one or all of the equations contain all of the variables we seek to solve. This method is initially supplied with an initial guess for all of the variables and by successive approximations, a better value for the variables are calculated until all of the

equations are close to zero, with the tolerance specified by the user. Because the equations are nonlinear and highly coupled, the initial guesses must be sufficiently close to the correct answer or the method will diverge and no solution will be found.

In the Newton-Raphson method, a Taylor series expansion is performed around an initial guess

$$g(c) = g(c^*) + \left.\frac{dg}{dc}\right|_* (c - c^*) + \cdots \qquad [1.57]$$

Higher order terms may be neglected because they influence the value of the equation very little. This yields a change variable

$$c - c^* = \Delta c = -\frac{g(c^*)}{dg/dc|_*} \qquad [1.58]$$

which is added to the previous value of the variable to give a closer approximation to the true value. This is expanded to a matrix form to solve all of the equations at once. As an example, the flash calculation in matrix form is shown in figure 3 below.

$$\begin{bmatrix} \frac{dg_1}{dk_{co_2}} & \frac{dg_1}{dk_{h_2o}} & \frac{dg_1}{dk_{meoh}} & \frac{dg_1}{dy_{co_2}} & \frac{dg_1}{dy_{h_2o}} & \frac{dg_1}{dy_{meoh}} & \frac{dg_1}{dx_{co_2}} & \frac{dg_1}{dx_{h_2o}} & \frac{dg_1}{dx_{meoh}} & \frac{dg_1}{dV} \\ \vdots & & & & & & & & & \\ \frac{dg_{10}}{dk_{co_2}} & \frac{dg_{10}}{dk_{h_2o}} & \frac{dg_{10}}{dk_{meoh}} & \frac{dg_{10}}{dy_{co_2}} & \frac{dg_{10}}{dy_{h_2o}} & \frac{dg_{10}}{dy_{meoh}} & \frac{dg_{10}}{dx_{co_2}} & \frac{dg_{10}}{dx_{h_2o}} & \frac{dg_{10}}{dx_{meoh}} & \frac{dg_{10}}{dV} \end{bmatrix} \begin{bmatrix} dk_{co_2} \\ dk_{h_2o} \\ dk_{meoh} \\ \vdots \\ dV \end{bmatrix} = \begin{bmatrix} g_1 \\ g_2 \\ g_3 \\ \vdots \\ g_{10} \end{bmatrix}$$

Figure 3: Diagram of the Newton-Raphson method applied to a flash calculation

In figure 3, g1 through g10 correspond to equations 1.34 through 1.37. These matrices can be approximated as

$$Ax = b \quad [1.59]$$

and the change variables, x, may be found by

$$x = A^{-1} \cdot b \quad [1.60]$$

where A^{-1} is the inverse of the A matrix. In the model, there are as many equations as mesh points, multiplied by the number of equations. A similar procedure as explained above is used to solve all of the equations for models 1 and 2. The inverse of the square matrix A, which contains all of the partial derivatives, is multiplied by a column vector b, which is the value of the equations at the current iteration at each mesh point. The negative of the change variable is added to the previous value to yield a closer approximation to the real value. The system of equations is converged when all of the values of b are close to zero.

Chapter 2: Model Structure

2.1 Finite Difference Scheme

Figure 4 shows where each of the six governing equations is solved in the GDL.

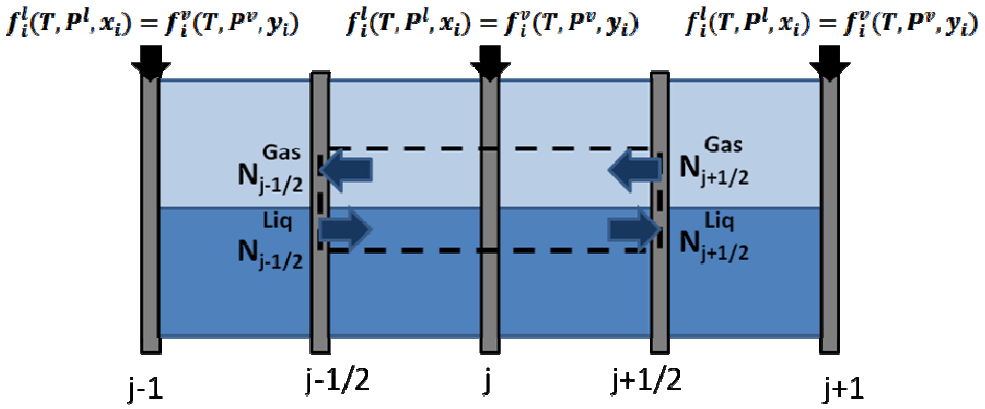

Figure 4: Grid of the GDL showing where each governing equation is solved

In order to solve the all of the six equations at once, the GDL is divided into a number of cells. On each side of the cell there is a mesh point, designated as j in figure 4. The thickness of the cell in the GDL is the same. As stated in section 1.7.2, the fluxes are defined at half mesh points. In order to do this, all of the six main variables and the variables which depend on them have to be defined at half mesh points on both the left (j-1/2) and the right (j+1/2) side of each interior mesh point when used in these equations. The result of this is that within each continuity equation (equations 1.46, 1.47, and 1.48), each one of the six variables used depends on the value at the mesh point to the left and right of it. This leads to tridiagonal portions in the partial derivative matrices.

Also as illustrated in figure 4, all of the equilibrium relations are defined at full mesh points, therefore the variables to the left and right of the mesh point do not influence the equilibrium relations.

2.2 BOUNDARY CONDITIONS

2.2.1 Model 1

In model 1, the boundary conditions at the fuel channel and GDL interface are the specification of the values of the three variables entering the GDL. These are the gas phase pressure, liquid phase pressure, and concentration of methanol. At the GDL and catalyst interface, the boundary conditions are as follows:

$$N_{CO_2} = -\frac{i}{6F} \quad [2.1]$$

$$N_{H_2O} = \frac{i}{6F} + \frac{i\xi_{H_2O}}{F} \quad [2.2]$$

$$N_{MeOH} = \frac{i}{6F} + \frac{i\xi_{MeOH}}{F} + \frac{D_{MeOH}C_{MeOH}}{L} \quad [2.3]$$

$$\xi_{MeOH} = 2.5x_{MeOH}$$

These boundary conditions for each species are taken from Faraday's law which states that the flux of each species is proportional to the current, i, produced dived by the number of electrons multiplied by Faraday's constant. In equation 2.2 and 2.3, the ξ is the electro-osmotic drag coefficient across the membrane from the anode catalyst layer to cathode catalyst layer. The drag coefficient of MeOH is much less than that of H_2O so it was assumed to be 2.5 times the mole fraction of methanol as stated in equation 2.3 [5]. In addition, the MeOH diffuses across the membrane to the cathode catalyst layer because of a concentration gradient. The L in equation 2.3 is the thickness of the membrane. It is assumed that the MeOH concentration at the cathode catalyst layer is zero because once it reaches it, it reacts with the excess oxygen at the cathode, leading to a mixed potential.

2.2.2 Flash Calculation

The inputs for a flash calculation are the liquid and gas pressures, and the overall composition of the inlet liquid feed mixture. Since the model is for a steady state DMFC, it was assumed that the inlet feed composition of CO_2 is its saturation value in H_2O and the composition of MeOH is the molar concentration or mole fraction desired.

2.2.3 Model 2

The boundary conditions at the fuel channel and GDL interface are the specification of the values of the six variables (section 1.7.2). These variables are the liquid and gas phase pressures and the liquid and gas phase mole fractions for CO_2 and H_2O. These variables are found by performing a flash calculation. If these boundary conditions aren't found by a flash calculation, the species aren't in true chemical equilibrium and there will be sharp discontinuity between the first and second node for the variables. This will prevent the model from finding the correct solution. At the GDL and catalyst interface, the boundary conditions are similar to those for model 1 and are as follows:

$$N^{l}_{CO_2} + N^{g}_{CO_2} = -\frac{i}{6F} \quad [2.4]$$

$$N^{l}_{H_2O} + N^{g}_{H_2O} = \frac{i}{6F} + \frac{i\xi_{H_2O}}{F} \quad [2.5]$$

$$N^{l}_{MeOH} + N^{g}_{MeOH} = \frac{i}{6F} + \frac{i\xi_{MeOH}}{F} + \frac{D_{MeOH}x_{MeOH}}{LV_{liq}} \quad [2.6]$$

$$\xi_{MeOH} = 2.5x_{MeOH}$$

$$x_{CO_2}\varphi^{l}_{CO_2}P^{l} = y_{CO_2}\varphi^{v}_{CO_2}P^{v} \quad [2.7]$$

$$x_{H_2O}\varphi^{l}_{H_2O}P^{l} = y_{H_2O}\varphi^{v}_{H_2O}P^{v} \quad [2.8]$$

$$x_{MeOH}\varphi^{l}_{MeOH}P^{l} = y_{MeOH}\varphi^{v}_{MeOH}P^{v} \quad [2.9]$$

Equations 2.4, 2.5, and 2.6 state the sum of the fluxes in the liquid and gas phases equals the flux from Faraday's law as well as the contributions due to electro-osmotic drag and diffusion across the membrane. In these equations, the catalyst layer is condensed into a boundary condition. Equations 2.7, 2.8, and 2.9 state that at the boundary, the species in the liquid and gas phases are in equilibrium.

2.3 CONVERGENCE

The model is converged when all of the equations defined at their respective mesh points and written in the form of equation 1.56 are below a specified tolerance. Convergence is not always guaranteed in the Newton Raphson method used. The user supplies initial guesses to the six main variables in the model and these guesses must be close to the expected values. If they aren't, the model will diverge. When using flash calculations, if the initial guesses aren't very close to the actual values, the values returned may be erroneous or have imaginary parts to them, which is nonphysical.

There are convergence issues in models 1 and 2 with respect to saturation. In DMFC operations, the liquid saturation value at the fuel channel/GDL interface is 1. It is not possible to have a saturation value of 1 when running simulations because it would force the gas permeability, equation 1.8, to 0. Therefore when simulations were run, the inlet saturation value was made as close as possible to 1, which was usually a value approximately equal to .95. The saturation depends on the user supplied liquid and gas phase pressures through equations 1.3 and 1.4.

If there is large spread in values in the jacobian matrix or in the matrix of equations (section 1.8.3), Matlab will give an error that the matrix is poorly conditioned. To avoid this error, equations 1.49, 1.50, and 1.51 were transformed to

$$ln\left(x_{CO_2}\varphi^{l}_{CO_2}P^{l}\right) = ln\left(y_{CO_2}\varphi^{v}_{CO_2}P^{v}\right) \qquad [2.7]$$

$$ln\left(x_{H_2O}\varphi^{l}_{H_2O}P^{l}\right) = ln\left(y_{H_2O}\varphi^{v}_{H_2O}P^{v}\right) \quad [2.8]$$

$$ln\left(x_{MeOH}\varphi^{l}_{MeOH}P^{l}\right) = ln\left(y_{MeOH}\varphi^{v}_{MeOH}P^{v}\right) \quad [2.9]$$

2.4 MATERIAL PROPERTY DATA

A large number of material property data are used to run the model and are given in Appendix A. These data were taken from various sources in the literature dealing with DMFC modeling and vapor-liquid equilibrium with conditions similar to the ones modeled here. These data enabled the simulation of the DMFC anode with various temperatures and feed compositions.

Chapter 3: Results

3.1 MODEL 1

The performance of the DMFC was analyzed in model 1 by changing some of the physical properties of anode and observing the effect on the gas phase pressure across the GDL and MeOH concentration at the GDL. Since current and potential aren't included in the model, the performance is judge by how high the gas phase pressure is, which would enable the removal of carbon dioxide, and how low the MeOH concentration is at the catalyst layer, which would reduce the MeOH crossover and mixed potential at the cathode.

Most GDLs are composed of carbon paper or some form. The following table shows parameters typical of carbon paper GDLs

Property	Value
Characteristic radius, r_o	6 μm
Characteristic spread, s	0.25
Absolute Permeability	$2x10^{-15}$ m^2
Contact Angle	45°

Table 1: Carbon paper GDL parameters

The following graphs show the variation of the three main variables across the GDL at 500 A/m^2, a temperature of 60°C, a 1 molar MeOH concentration, and a saturation value of .95 at the fuel channel and GDL interface.

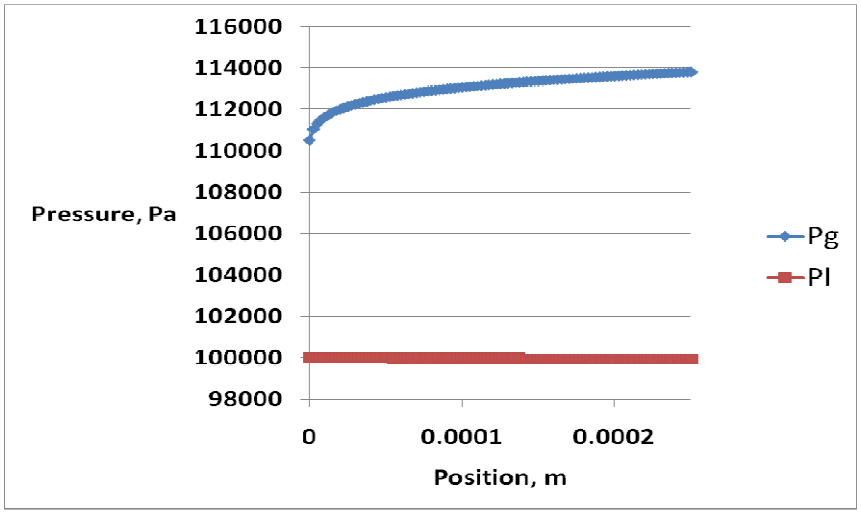

Figure 5: Liquid and gas phase pressure profiles

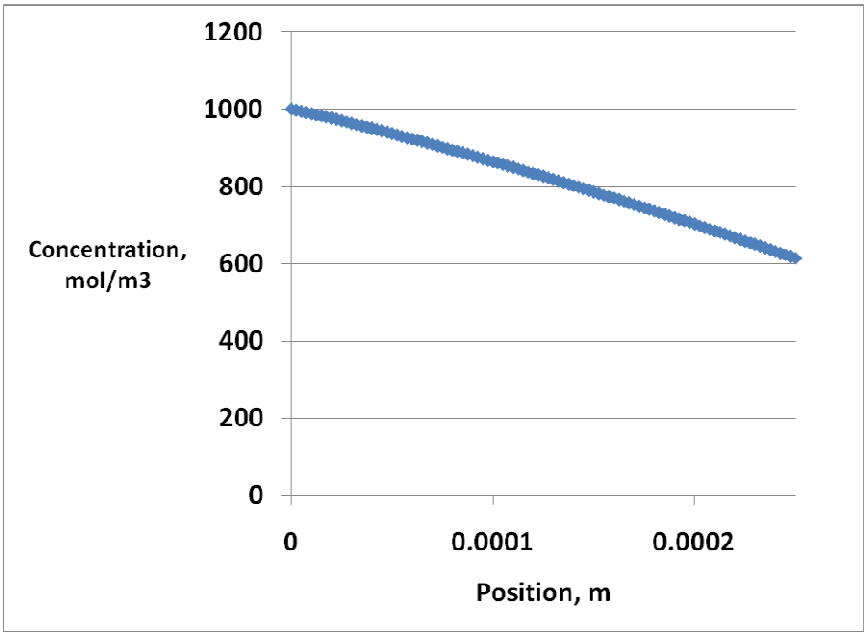

Figure 6: Methanol concentration profile

Figure 5 shows that the both and liquid and gas phase pressures vary linearly across the GDL. There is a sharp increase in the gas pressure at the fuel channel and GDL interface which is proportional to

$$\frac{1}{(1-S_n)} \qquad [3.1]$$

which can be found from equations 1.11 and 1.7. In order to remove the CO_2 from the GDL, there must be a significant positive pressure gradient. Also shown in figure 5 is that there is only a small negative liquid pressure variation across the GDL.

Figure 6 shows that the there is a linear methanol concentration across the GDL. As the current increases, the profile becomes more steep until the concentration gets driven down to zero.

In the following sections, the effect of varying some of the parameters has on the performance of the anode will be shown.

3.1.1 Contact Angle

The effect of varying the contact angle on the methanol concentration at the catalyst layer is shown in Figure 7.

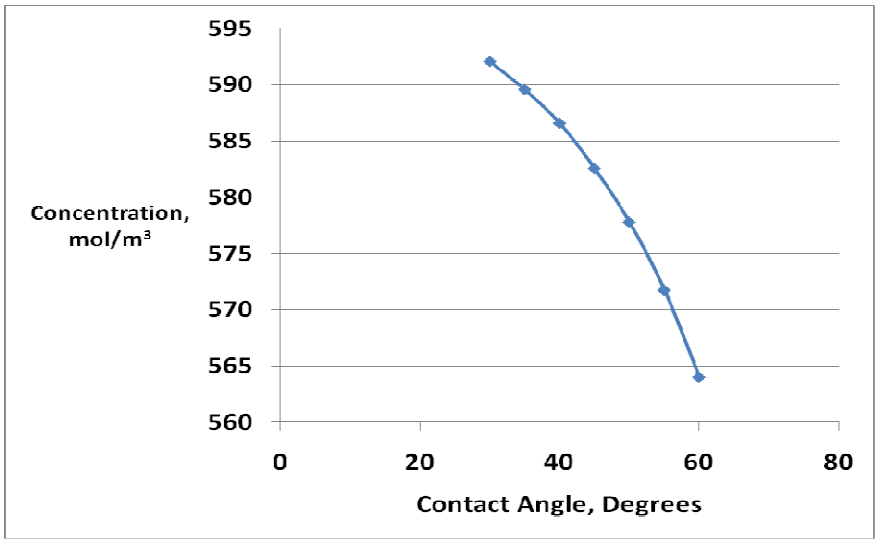

Figure 7: Effect of contact angle on the MeOH concentration at the catalyst layer

As shown in figure 7, as the contact angle increases, the methanol concentration decreases at the anode catalyst layer. The contact angle can be thought of as the wettability of the GDL [21]. The smaller the contact angle, the more wettable the surface

of the GDL is, meaning it is easier for a solution like MeOH and H_2O to spread across its surface. To make the surface of the GDL more wettable, hydrophilic materials like Nafion are usually added to the GDL. In contrast, to make the surface of the GDL more less wettable, hydrophobic materials like PTFE (teflon) are usually added to the GDL. Therefore in figure 7, as the contact angle increases, meaning as the GDL becomes more hydrophobic, the concentration of methanol at the catalyst layer decreases because it becomes more difficult for the liquid solution to flow.

The effect of varying the contact angle on the gas pressure difference across the GDL is shown in figure 8.

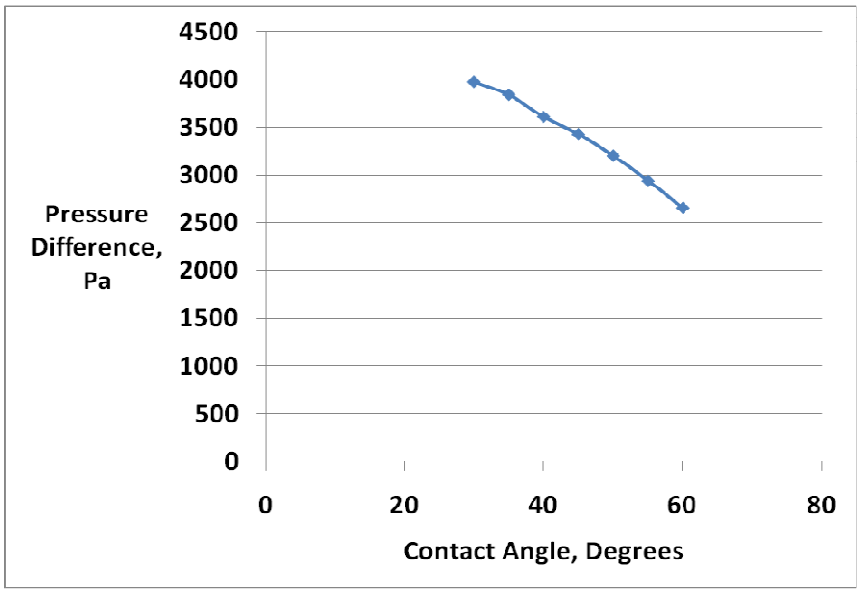

Figure 8: Effect of contact angle on the gas pressure difference across the GDL

The velocity of the gas is proportional to the gradient in gas pressure (equation 1.13). Therefore a large gas pressure difference between the fuel channel/GDL interface and the GDL/catalyst layer interface would mean a large overall velocity for the gas to exit. Figure 8 shows that as the contact angle increases, the gas pressure difference, and hence the velocity of the gas, decreases. Figure 8 shows the importance of two phase flow in

CO_2 gas removal. As the GDL becomes more wettable, both the flow of liquid and gas is enhanced.

From figure 6 and 7 there appears to be a trade off between removing carbon dioxide and lowering the methanol concentration at the catalyst layer. Increasing the contact angle while holding the other parameters of the GDL constant lowers the pressure difference across the GDL while decreasing the methanol concentration at the catalyst layer.

3.1.2 Absolute Permeability

The effect of varying the absolute permeability of the GDL on the methanol conentration at the catalyst layer is shown in figure 9.

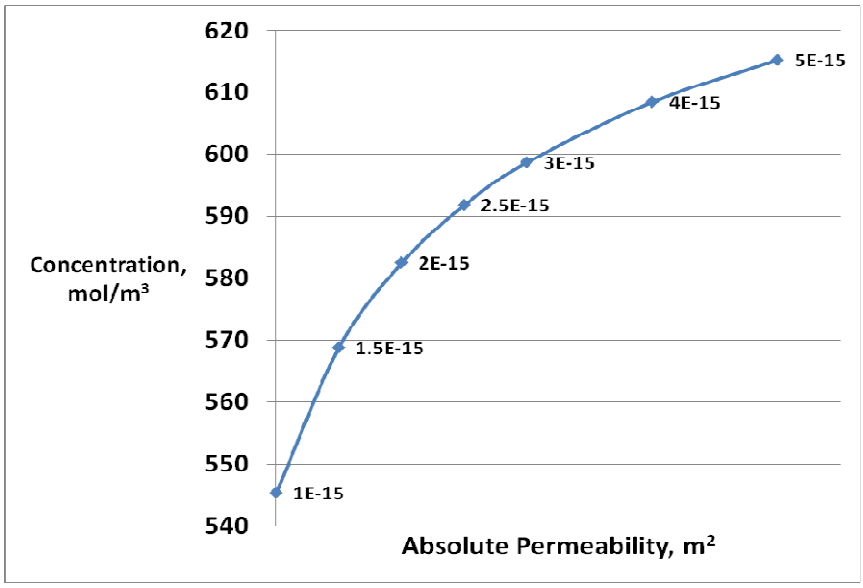

Figure 9: Effect of absolute permeability on methanol concentration at catalyst layer

Increasing the absolute permeability of the GDL results in an increase in the methanol concentration at the catalyst layer. Permeability is the measure of the ability of a porous

material to transmit a fluid. From increasing the absolute permeability, figure 9 shows that the liquid velocity is increased, hence an increase in methanol concentration.

The effect of varying the absolute permeability of the GDL on the gas pressure difference across the anode is shown in figure 10.

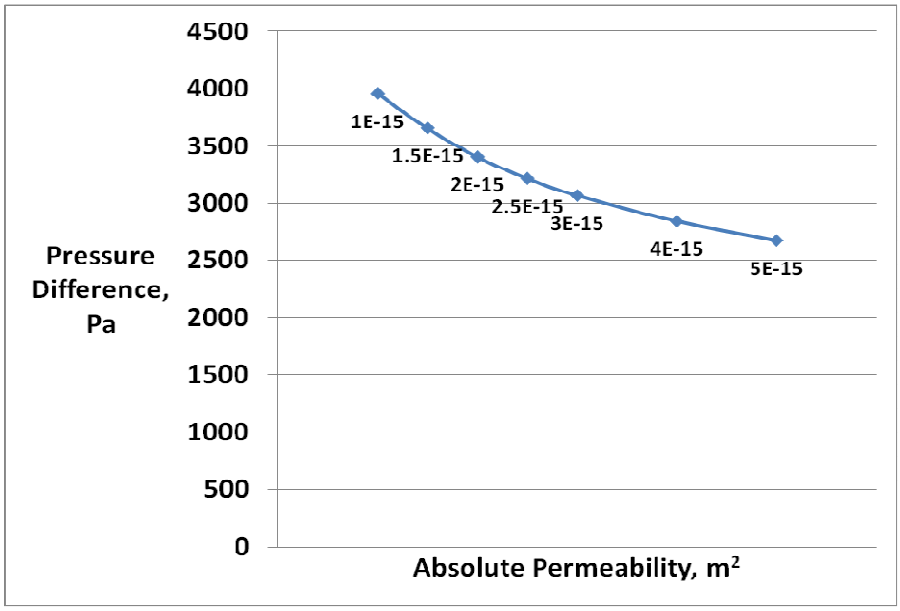

Figure 10: Effect of absolute permeability on the gas pressure difference across the GDL

As the absolute permeability of the GDL increases, the gas pressure difference across the anode decreases. As the permeability increases, it is easier for the liquid phase to be transported to the catalyst layer, however this may hinder the transport of the gas phase in the opposite direction.

Varying the absolute permeability of the GDL has a better effect on controlling both the gas velocity and methanol concentration simultaneously than the varying the contact angle. A small permeability, in the range of $1x10^{-15}$ m^2, can enhance the ability to remove CO_2 gas from the GDL while at the same time decreasing the MeOH concentration at the catalyst layer.

3.1.3 GDL Thickness

The effect of varying the thickness of the GDL on the MeOH conentration at the catalyst layer and the gas pressure difference across the GDL is shown in figures 11 and 12, respectively.

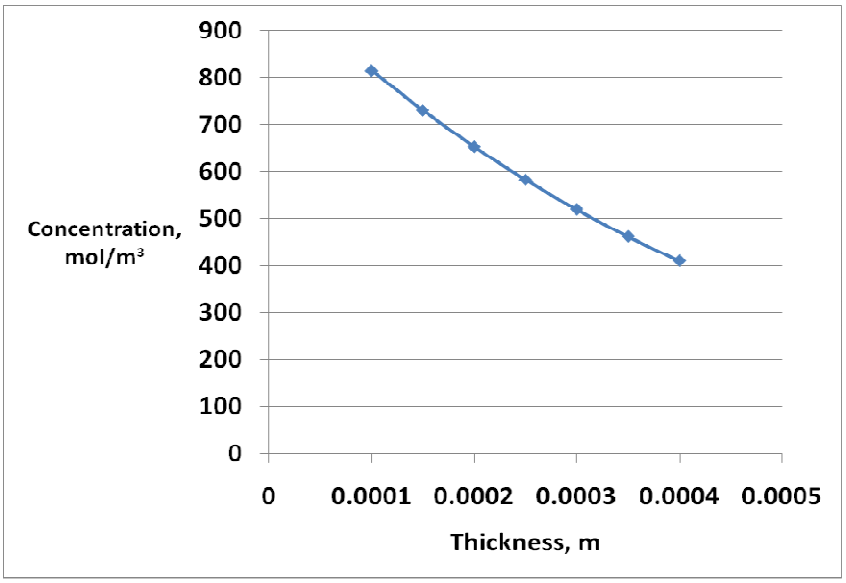

Figure 11: Effect of GDL thickness on methanol concentration at catalyst layer

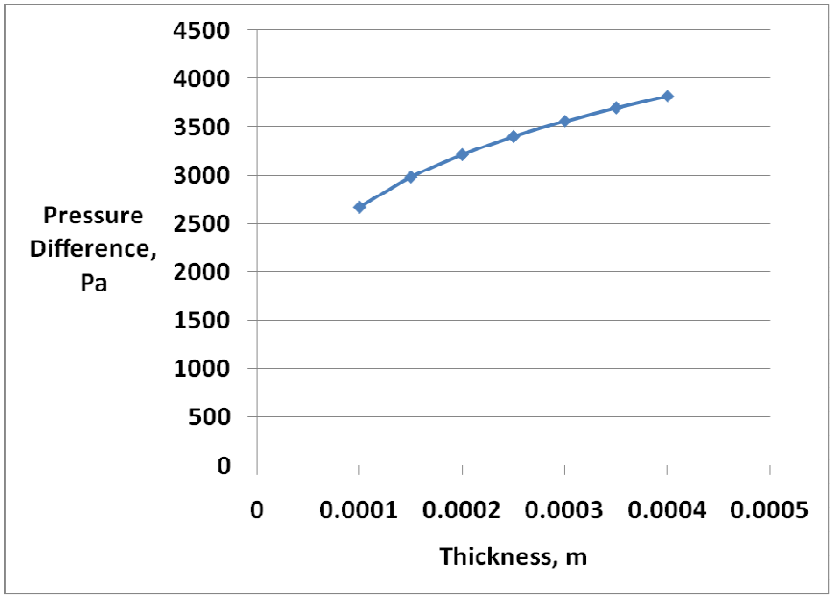

Figure 12: Effect of GDL thickness on the gas pressure difference across the GDL

Figure 11 shows that as the thickness of the GDL is increased, the concentration of MeOH at the catalyst layer decreases significantly. This is probably because as the thickness is increased, there is a corresponding increase in the liquid mass transfer resistance. Figure 12 shows that as the thickness of the GDL is increased, the gas pressure difference across the GDL increases as well. This is probably due to a larger gradient in pressure needed to force the gas out a farther distance.

Increasing the thickness of the GDL both lowers the MeOH concentration at the catalyst layer while increasing the gas velocity for removing of the CO_2. A larger gas pressure gradient has to be formed in order to move the CO_2 gas a farther distance. However, there may be a danger of completely blocking some of the pores with gas as the thickness of the GDL is increased. This is because as the thickness is increased, the liquid saturation decreases. This effect is shown in figure 13.

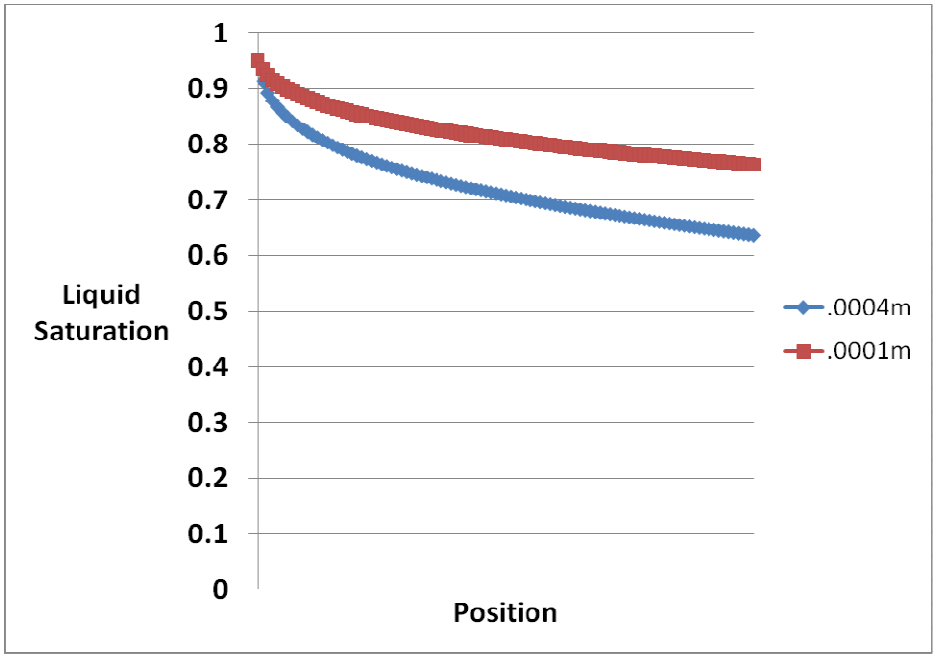

Figure 13: Comparison of saturation profiles for two different GDL thicknesses

Figure 13 shows that as the thickness of the GDL increases, the liquid saturation decreases. At the catalyst layer interface, there is more gas occupying the pores which would limit the amount of MeOH reaching the catalyst layer, thereby decreasing MeOH crossover. However, there is a danger that the gas could block portions of the surface of the catalyst layer causing an uneven distribution of MeOH which would lower the fuel cell's performance.

3.2 FLASH CALCULATION

In order to accurately describe equilibrium between the phases, a flash calculation is used. It is used in model 2 to output the mole fractions of each species in each phase as well as the fugacity coefficients. The variation of the gas phase mole fractions are shown in figure 14. The overall composition is 95% H_2O, 4.5% MeOH, and .5% CO_2. The liquid phase mole fractions vary little with temperature.

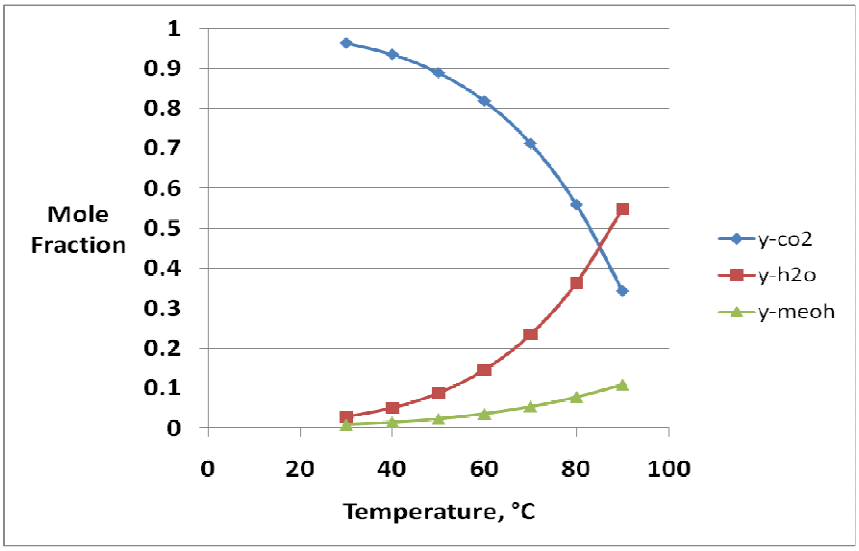

Figure 14: Variation of the mole fraction of the gas species with temperature

Figure 14 shows that at low temperatures, most of the gas phase is composed of CO_2. As the temperature increases, the mole fraction of CO_2 decreases and the mole fractions of H_2O and MeOH increase. At high operating temperatures, the mole fraction of H_2O becomes the largest mole fraction in the gas phase and significant amounts of MeOH vapor are present. This is because we are approaching the boiling point of MeOH, The novelty of model 2 is its use of a flash calculation to describe equilibrium in the presence of a capillary pressure. Most DMFC models use simplifying assumptions or correlations to calculate the concentration, Henry's law constant, and partial pressure of the species in equilibrium. These correlations usually only depend on the temperature. Partial pressure, and hence equilibrium, depends on the temperature and the overall mixture composition.

To compare the mole fractions predicted by the SRK equation of state, the Peng-Robinson (PR) equation of state was used. The equations for the PR equation of state are

given in Appendix B. Figures 15 and 16 show the K-values (equation 1.34) predicted by each equation of state.

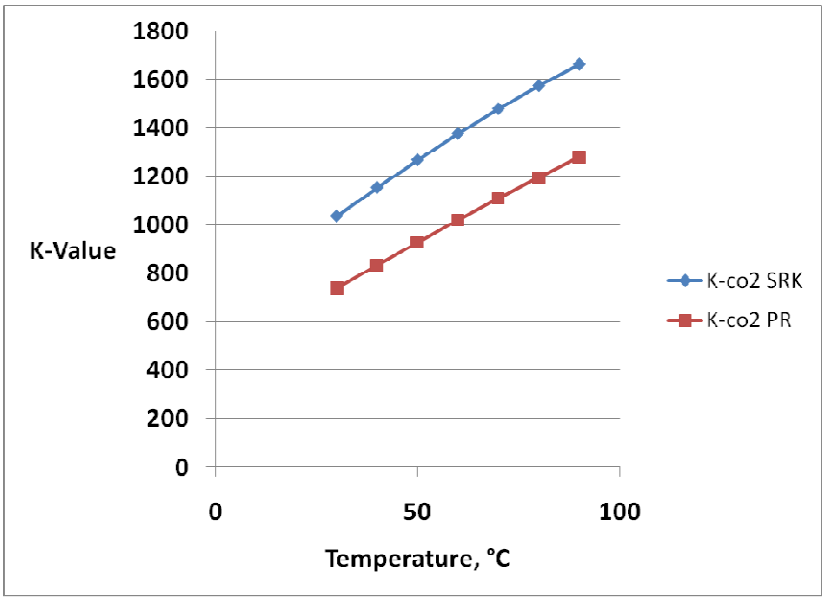

Figure 15: Comparison of the CO_2 K-value predicted by the SRK and PR equations of state

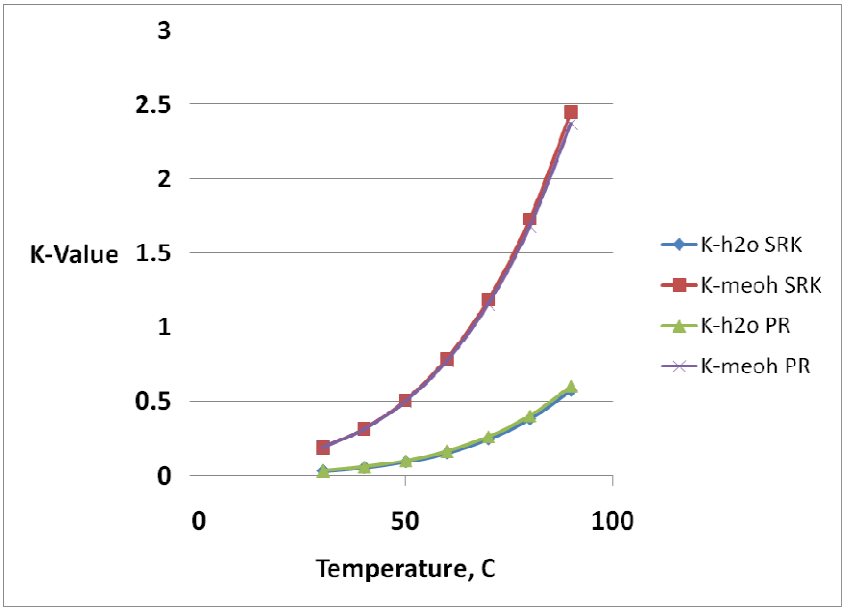

Figure 16: Comparison of the H_2O and MeOH K-values predicted by the SRK and PR equations of state

Figures 15 and 16 show that the trends predicted by each equation of state are similar. The K-values predicted by each equation of state are close one another for H2O and MeOH. For CO2, the SRK equation of state predicts a much higher mole fraction ratio than the PR equation of state for all temperatures, but the trend is similar. The SRK equation of state predicts a significantly smaller liquid mole fraction for CO_2, but on the same order.

3.3 MODEL 2

Similarly to Model 1, the performance of the DMFC was analyzed in model 2 by changing some of the physical properties of anode and observing the effect on the gas phase pressure across the GDL, the MeOH mole fraction at the GDL, and the partial pressure of MeOH at the fuel channel. Since current and potential aren't included in the model, the performance is judge by how high the gas phase pressure is, which would enable the removal of carbon dioxide, how low the methanol mole fraction is at the catalyst layer, which would reduce the MeOH crossover and mixed potential at the cathode, and the partial pressure of MeOH

The following graphs show the variation of the six main variables across the GDL at 600 A/m^2, a temperature of 30°C, a 2.5 molar MeOH concentration, and a saturation value of .94 at the fuel channel and GDL interface.

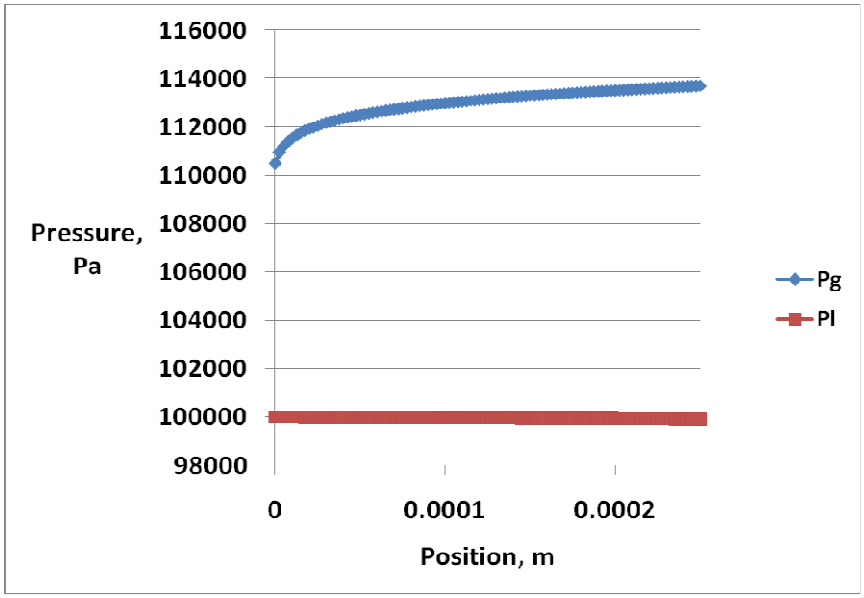

Figure 17: Liquid and gas phase pressure profiles across the GDL

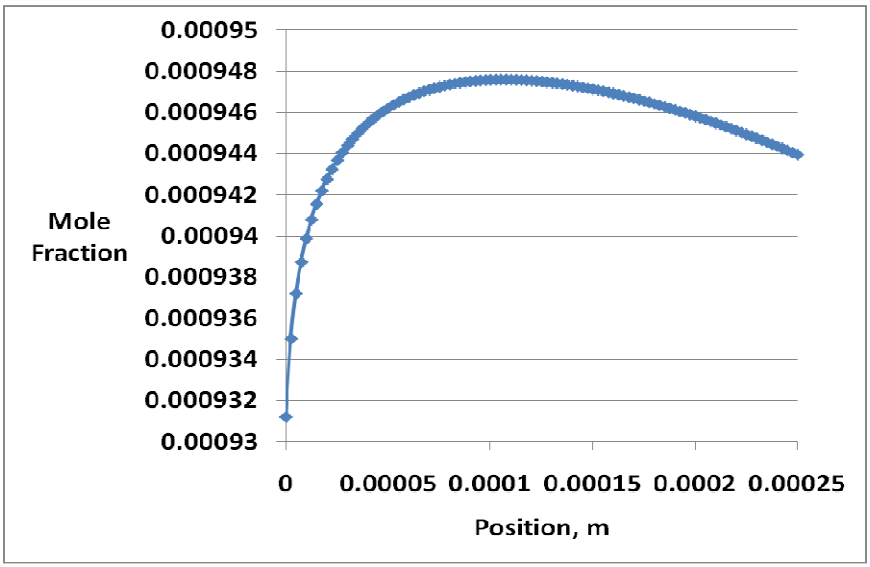

Figure 18: CO_2 liquid mole fraction across the GDL

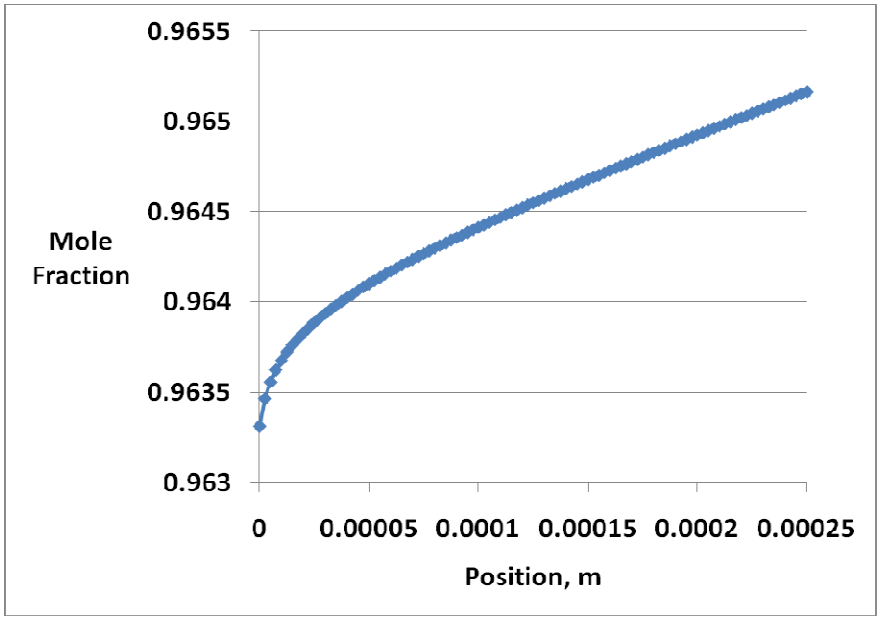

Figure 19: CO_2 gas mole fraction across the GDL

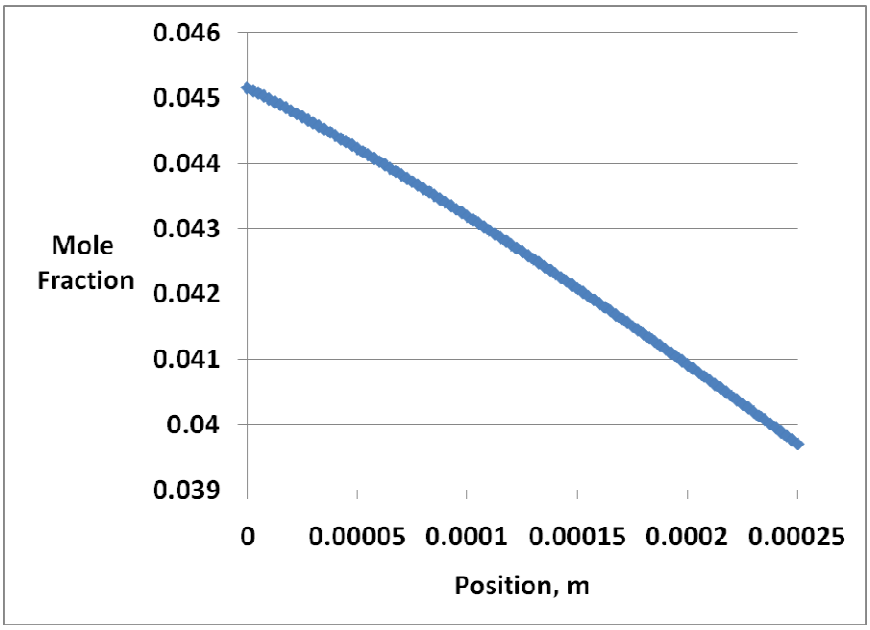

Figure 20: MeOH liquid mole fraction across the GDL

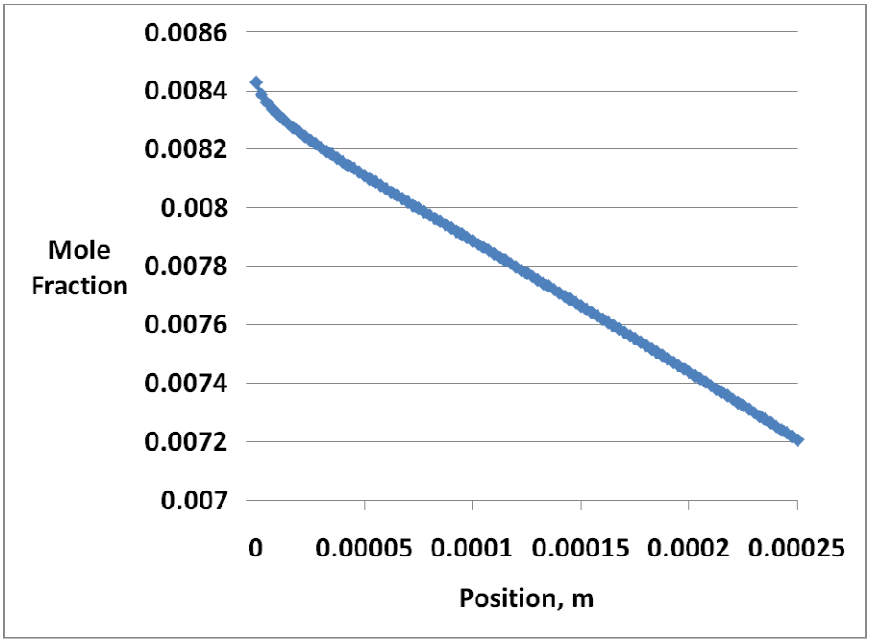

Figure 21: MeOH gas mole fraction across the GDL

Figure 17 shows that the liquid and gas phase pressures vary similarly to the liquid and gas phase pressures in model 1. There is little change in the liquid phase pressure and the gas phase pressure shows a sharp increase at the fuel channel boundary then increases linearly toward the catalyst layer. Figure 18 shows the CO_2 liquid phase mole fraction variation has a parabolic shape, and its mole fraction only increases slightly between the boundaries. It appears that liquid MeOH and H_2O are making the liquid phase less hospitable for CO_2 towards the catalyst layer. Figure 18 also shows that there is an accumulation of liquid CO_2 near the inlet. Figure 19 shows the CO_2 gas phase mole fraction increases approximately linearly across the GDL. Both the CO_2 liquid and gas phase increase approximately 1% across the GDL. Figures 20 and 21 show the liquid and gas phase mole fraction variation of MeOH across the GDL, respectively. The liquid phase mole fraction decreases 11% and the gas phase mole fraction decreases 14%. Therefore even at low operating temperatures, it is predicted that the MeOH gas phase

will carry a significant portion of the flux to the catalyst layer. Section 3.3.4 will show how this varies as the temperature is increased.

3.3.1 Contact Angle

The effect of varying the contact angle on the methanol concentration at the catalyst layer is shown in Figure 22.

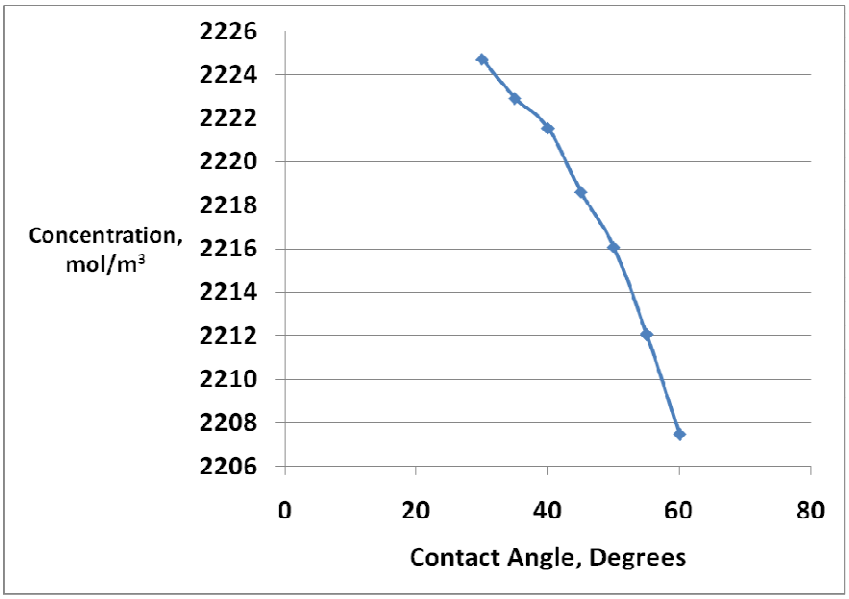

Figure 22: Effect of contact angle on the MeOH concentration at the catalyst layer

Similarly to model 1, figure 22 shows that as the contact angle is increased, the MeOH concentration at the catalyst layer is reduced. As the contact angle is increased, the wettability of the GDL is decreased and the internal resistance to the flow of the MeOH solution is increased. Therefore the concentration at the catalyst layer is reduced.

The effect of varying the contact angle on the methanol concentration at the catalyst layer is shown in Figure 23.

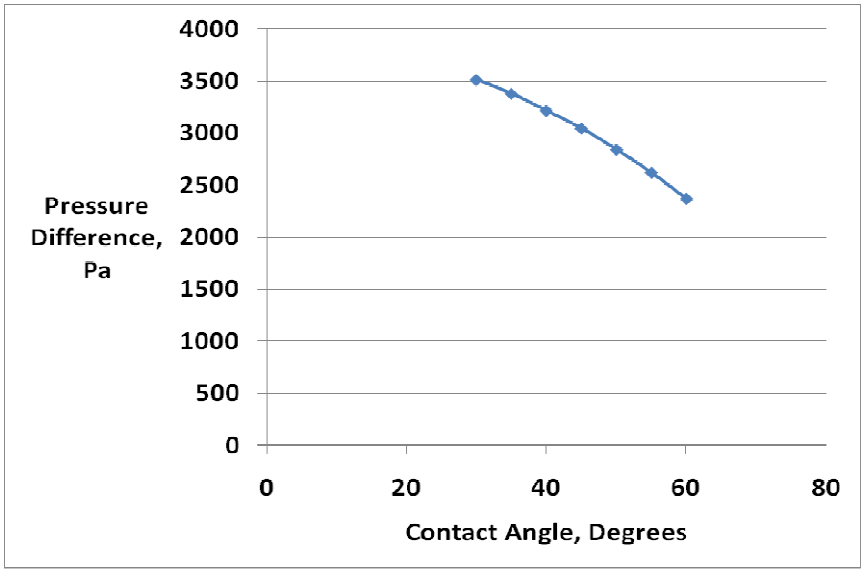

Figure 23: Effect of contact angle on the gas pressure difference across the GDL

Like in model 1, figure 23 shows that as the contact angle is increased, the pressure difference across the GDL decreases. This is most likely because as the contact angle is increased, the GDL becomes more hydrophobic. Presumably, as the GDL becomes more hydrophobic, the gas phase has specific channels or paths to flow through from the catalyst layer to the fuel channel, enhancing its transport. However, these hydrophobic portions become filled with liquid MeOH solution, hindering the gas phase from exiting the GDL. A large gas phase pressure gradient is needed to remove the gas mixture and prevent the blocking of pores.

3.3.2 Absolute Permeability

The effect of varying the absolute permeability of the GDL on the MeOH concentration at the catalyst layer is shown in Figure 24.

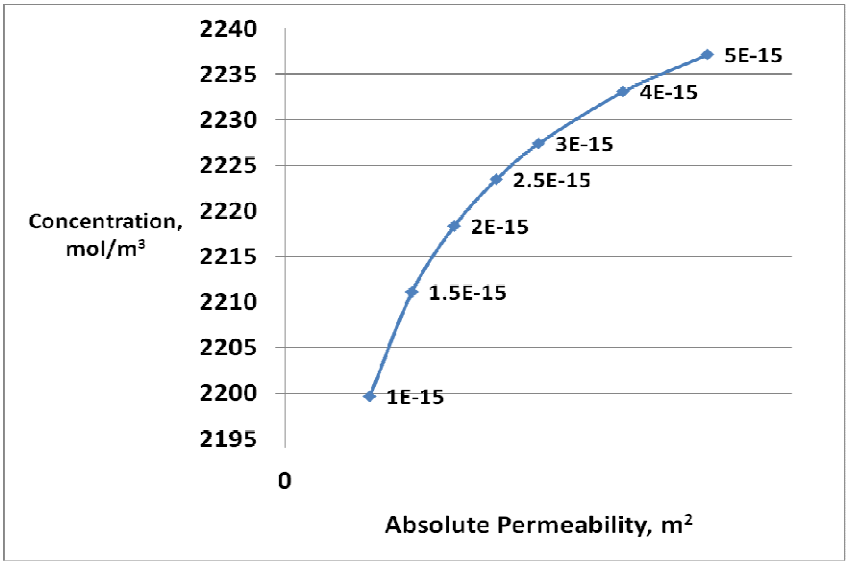

Figure 24: Effect of varying the absolute permeability on the MeOH concentration at the catalyst layer.

Figure 24 shows the same trend predicted by model 1. As the absolute permeability of the GDL is increased, the methanol concentration at the catalyst layer is increased. Increasing the permeability increases the liquid flow rate, causing a higher concentration to be present at the catalyst layer. This would presumably increase the possibility of MeOH crossover from the anode catalyst layer to the cathode catalyst layer since a higher methanol concentration is present. The difference between model 1 and model 2 is that model 1 predicts a much higher percent increase (13%) in the liquid MeOH concentration from increasing the permeability from $1x10^{-15}$ m^2 to $5x10^{-15}$ m^2. This is because all of the MeOH is present in liquid form in model 1, whereas it is split between the liquid and gas phases in model 2.

The effect of varying the absolute permeability of the GDL on the gas pressure difference is shown in Figure 25.

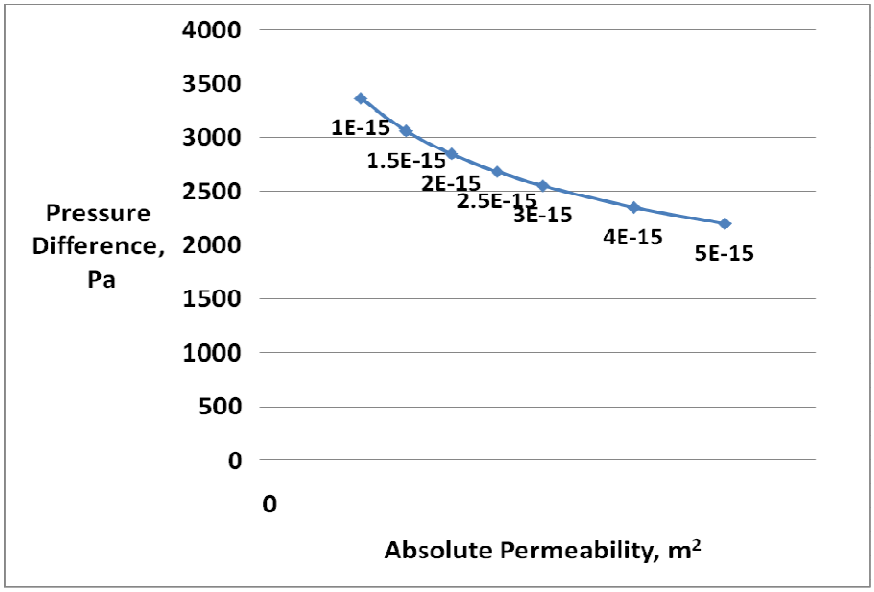

Figure 25: Effect of varying the absolute permeability on the gas pressure difference across the GDL.

The effect of varying the absolute permeability on the gas pressure difference across the GDL predicted by model 2 is similar to that predicted by model 1. As the permeability increases, the gas pressure difference decreases. This is because the increase in permeability enhances the liquid phase transport to the catalyst layer while lowering the gas phase transport out of the GDL.

3.3.3 Bubble Detachment Size

Numerous studies have shown that small homogeneous bubbles on the back of the GDL increase the performance of the DMFC compared to large randomly distributed bubbles. The influence of the contact angle on the bubble detachment size is shown in figure 26.

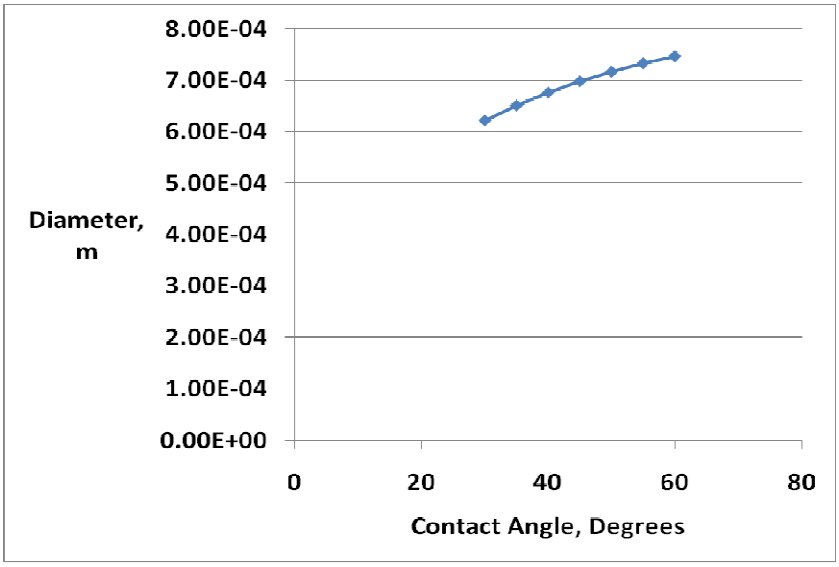

Figure 26: Effect of contact angle on the diameter of the detached bubble

As the contact angle is increased, the diameter of the detached bubble increases. The bubble detachment is a strong function of the contact angle or wettability as seen in equation 1.41. As the contact angle increases, the wettability decreases and the GDL becomes more hydrophobic. Therefore to produce smaller uniform bubbles, the GDL must be more hydrophilic as well as having a small characteristic radius.

3.3.4 Limiting Current Density

Model 1 and model 2 both predict the same overall trends in MeOH concentration and the gradient in gas pressure across the GDL, but their relative values differ. The largest difference between the models is the prediction of the limiting current density. Figure 27 shows the MeOH concentration profile for the limiting current density for model 1 with an inlet concentration of 1 molar.

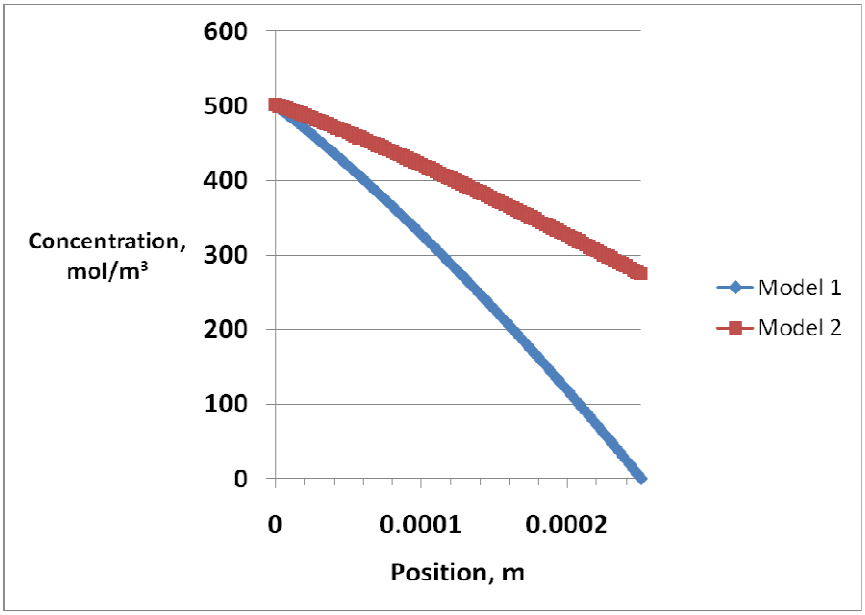

Figure 27: MeOH concentration profiles across the GDL for models 1 and 2 at model 1's limiting current density

The concentration profile in figure 27 is shown at a current density of 791.5 A/m^2. This is the current density needed to drive the MeOH concentration to zero between the GDL and CL. As shown in the figure, model 1 reaches a zero MeOH concentration at this current density while the concentration in model 2 is approximately 270 mol/m^3. The limiting current density for model 2 was found to be 2200 A/m^2, which is close to experimental values [14]. The disparity between the models stems from the combined two phase and equilibrium effects. Because MeOH liquid and gas are in equilibrium, both the liquid concentration of MeOH and the MeOH gas partial pressure have to driven down to zero in model 2, while only the the liquid MeOH has to be driven down to zero in model 1.

3.3.5 Flux at Boundary

In most models of the DMFC, especially single phase models and those which don't take equilibrium of the phases into account, it is believed that CO_2 in the gas phase and H_2O and MeOH in the liquid phases are the dominant fluxes at the GDL and catalyst layer interface. Because the mole fractions of CO_2 in the gas phase and H_2O in the liquid phase are several orders of magnitude larger than their respective mole fractions in the other phase, this is a reasonable assumption. However for MeOH, the mole fractions are on the same order, even at low temperatures. Figure 28 shows how the molar flux density of each phase varies at the catalyst layer interface.

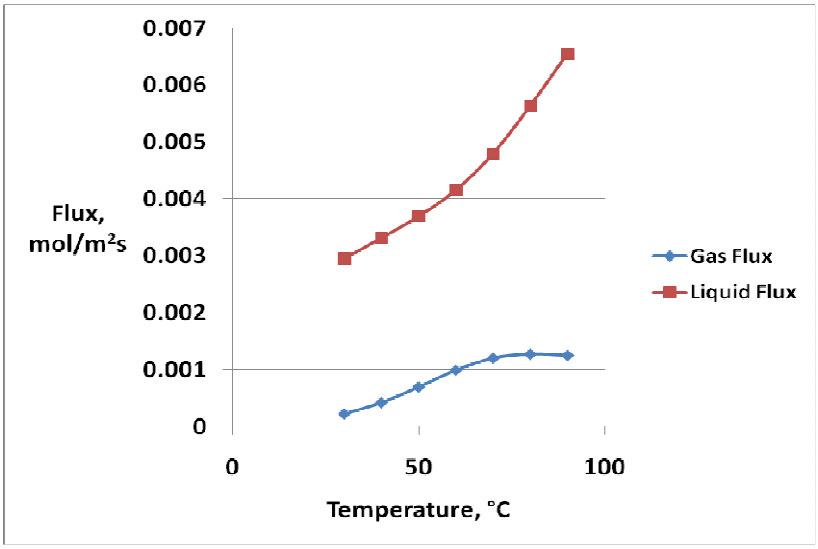

Figure 28: Effect of temperature on the flux of MeOH

Figure 28 shows that even at low temperatures, the flux density of MeOH for the liquid and gas phases are of the same order, with the liquid phase being the larger flux. As the temperature is increased, both the liquid and gas fluxes increase until about 70 °C where the gas flux levels out. This is because of the liquid and gas velocities. As the temperature is increased significantly, there is a peak in the gas pressure and it decreases

midway in the GDL towards the catalyst layer. This phenomenon happens at around 70 °C. This means the gas velocity is positive at this point. As the temperature increases past this point, the now positive gas velocity increases with increasing temperature, causing the peak in figure 28. The percent of the gas MeOH flux that makes up the total MeOH flux is shown in table 2.

Temperature, °C	Gas Flux Percent
30	7.2
40	11.4
50	15.9
60	19.3
70	20.1
80	18.4
90	16.1

Table 2: Percent of the gas MeOH contributing to the total flux of MeOH at the catalyst layer

Table 2 shows that the molar gas flux density of MeOH is a significant portion of the overall MeOH flux. As the temperature increases, the gas flux is predicted to contribute an increased amount until 70 °C where the percent begins to decrease. From figure 27 and table 2, it is shown that when modeling DMFCs, the MeOH vapor phase must be included.

3.3.6 Conclusions

From this research, several conclusions can be made about modeling and improving the performance of the DMFC anode.

In this study, the performance of the DMFC anode was judge as lowering the MeOH concentration at the anode catalyst layer to decrease methanol crossover from the anode to cathode catalyst layers and increasing the gradient in gas pressure across the

anode GDL to promote the removal of gas from the pores of the GDL. From the results, it appears that improving the performance of the DMFC is often a tradeoff.

To promote gas removal, it was found that having a small contact angle, a small absolute permeability, and a thick GDL will work. A small contact angle will enhance the ability of the liquid solution to spread over the porous surface of the GDL, reducing the mass transfer resistance of the liquid phase and at the same time, promoting increased two phase counter flow in the GDL. A small absolute permeability will also promote the gas phase removal from the GDL. A large permeability will enhance the liquid phase transport to the catalyst layer while hindering the counter flowing gas phase. Finally, a thicker GDL will also promote the removal of the gas phase. A thicker GDL will mean the gas phase pressure gradient will have to be larger to force the gas out.

Related to the CO_2 gas phase removal is that of bubble detachment. The easier it is for the bubbles to detach from the backing of the GDL, the better the DMFC will perform because the bubbles reduce the effect mass transport area of the GDL and also retard the solution flow in the fuel channels. Small homogenous bubbles are easier to remove from the backing compared to larger inhomogeneous ones. It was found that a smaller contact angle produces a smaller diameter on the detached bubble. Therefore hydrophilic GDLs will promote better bubble detachment.

To reduce MeOH concentration at the catalyst layer the GDL needs to have a large contact angle, a small absolute permeability, and to be thick. All three of these promote an increase in the liquid mass transfer resistance making it harder for the methanol solution to reach the catalyst layer.

From this analysis, having a small absolute permeability and a thick GDL would work best to both lower the MeOH concentration at the catalyst layer while also

promoting CO_2 gas removal. The contact angle would need to be tailored to a specific application.

It was also found that modeling the GDL based on simplified two phase flow not including equilibrium between the phases works well at predicting the general trends of DMFC dynamics. However it doesn't predict the importance of the species in other phases on the performance, particularly MeOH vapor. It also is poor at predicting the limiting current densities.

Realistically, improving the DMFC performance based on the above conclusions will not always give the expected results. There are contradictions in the literature with respect to what is needed for improved DMFC performance, especially with respect to contact angle. In some papers in the literature [20], researchers have found that having hydrophobic portions of the GDL promotes gas phase flow. In some applications, PTFE is added to the GDL to add hydrophobic pathways for the gas phase to exit. This was found to improve the performance of the DMFC. In other papers [21] [19], the conclusions agree with the results of the study which is hydrophilic GDLs increase the performance of the GDL. Clearly, further investigation needs to be performed to find the effect of the contact angle and the degree of hydrophilicity on the performance of the DMFC.

3.3.7 Other Model Uses

The set of governing equations for the GDL can be used in other ways to gauge the performance of the fuel cell.

As stated in the background, during operation of the DMFC, the fuel is recycled and becomes saturated with CO_2. During further operation, any CO_2 which is produced from the reaction at the catalyst layer is in the form of gas. This gas has to be removed from fuel channel or else it will lower the performance of the fuel cell. When this gas is

removed, H_2O and MeOH vapor is removed with it. From section 3.2, both H_2O and MeOH vapor are also present in the gas phase during steady state operation at all operating temperatures of interest. Since the gas phase has to flow out of the GDL into the fuel channel, there is a loss of H_2O and MeOH in the vapor phase because of convection even though their overall flux is toward the catalyst layer because of diffusion. The equations developed in model 2 can be used to predict the amount of MeOH vapor lost during operation from start up to steady state.

The model could also be used to predict limiting current densities for higher MeOH concentrations. Because the equations are highly coupled and nonlinear in nature, especially through the equilibrium relations, solution of these equations at high current densities would require close initial guesses.

The model can be used to predict the effect MeOH vapor has on the performance of the DMFC at a range of temperatures. Specifically, the model can be extended to the anode catalyst layer to elucidate the effect the MeOH vapor has on MeOH crossover.

Finally, the model can be used in system level modeling. If the MeOH crossover can be reduced by increasing the mass transfer resistance of the MeOH through the GDL using the results presented in the preceding sections, then a higher concentration of MeOH can be used. This means a smaller tank will be needed for portable electronic devices.

Appendix A Material Property Data

The material property data for the models are given below with the symbols and references for each value, were applicable.

A.1 GDL Properties

Parameter	Symbol	Value	Reference
Characteristic Radius (μm)	r_o	6	[25]
Characteristic Spread	s_k	0.25	[25]
Bulk Porosity	ε_o	0.6	[25]
Absolute Permeability (m^2)	K_{sat}	$2x10^{-15}$	[25]
Contact Angle	θ	45°	[25]

A.2 Fluid Properties

Parameter	Symbol	Value	Reference
Water Surface Tension (N/m)	γ	0.06606	[25]
Water Viscosity (Pa-s)	μ_{H2O}	$.65x10^{-3}$	[43]
CO_2 Viscosity (Pa-s)	μ_{CO2}	$1.626x10^{-5}$	[5]
Water Molar Volume (mol/m^3)	V^l_{H2O}	$1.8016x10^{-5}$	[37]

A.3 Diffusion Coefficients

Symbol	Value	Reference
$D_{MeOH,H2O}$ Liq	$6.69x10^{-9}$	[11]
$D_{CO2,H2O}$ Liq	$3.67X10^{-9}$	[43]
$D_{MeOH,H2O}$ Gas	$(-6.954x10^{-2}+4.5986xTx10^{-4}+9.4979xT^2 10^{-7})x10^{-4}$	[44]
$D_{MeOH,CO2}$ Gas	$(-6.954x10^{-2}+4.5986xTx10^{-4}+9.4979T^2x10^{-7})x10^{-4}$	[44]
$D_{CO2,H2O}$ Gas	$2.56x10^{-5}(T/307)^{2.334}*((1.013*10^5)/165000)$	[45]
D_{MeOH} in Nafion	$4.9x10^{-10}xe^{2436x(1/333-1/T)}$	[42]

All diffusion coefficients have units of (mol/m^2s)

A.4 Uniquac Parameters

Van der waals volume and area parameters as well as acentric factors for the species.

Symbol	Value	Reference
V_{wCO2} (m^3/kmol)	$1.97x10^{-2}$	[37]
V_{wH2O} (m^3/kmol)	$1.237x10^{-2}$	[37]
V_{wMeOH} (m^3/kmol)	$2.171x10^{-2}$	[37]
A_{wCO2} (m^2/kmol)	$3.23x10^{8}$	[37]
A_{wH2O} (m^2/kmol)	$2.26x10^{8}$	[37]
A_{wMeOH} (m^2/kmol)	$3.58x10^{8}$	[37]
ω_{CO2}	0.225	[37]
ω_{H2O}	0.3438	[37]
ω_{MeOH}	0.56533	[37]

A.4a SRK Binary Interaction Parameters

Symbol	Value	Reference
$\Delta u_{CO2\text{-}H2O}$ (K)	777	[36]
$\Delta u_{H2O\text{-}CO2}$ (K)	304	[36]
$\Delta u_{MeOH\text{-}H2O}$ (K)	186	[36]
$\Delta u_{H2O\text{-}MeOH}$ (K)	-104.18	[36]
$\Delta u_{MeOH\text{-}CO2}$ (K)	68	[36]
$\Delta u_{CO2\text{-}MeOH}$ (K)	156	[36]

A.4b Peng Robinson Binary Interaction Parameters

Symbol	Value	Reference
$\Delta u_{CO2\text{-}H2O}$ (K)	998	[36]
$\Delta u_{H2O\text{-}CO2}$ (K)	328	[36]
$\Delta u_{MeOH\text{-}H2O}$ (K)	-180	[36]
$\Delta u_{H2O\text{-}MeOH}$ (K)	289	[36]
$\Delta u_{MeOH\text{-}CO2}$ (K)	108	[36]
$\Delta u_{CO2\text{-}MeOH}$ (K)	124	[36]

A.5 Base Case and Operating Conditions

Parameter	Value	Reference
GDL Thickness (m^2)	$2.5x10^{-4}$	Assumed
Membrane Thickness (m^2)	$2.5x10^{-4}$	Assumed
Operating Temerature (K)	303.15	Assumed
Liquid Phase Pressure (Pa)	$1x10^5$	Assumed
MeOH Concentration (mol/m^3) - Model 1	1000	Assumed
H_2O Concentration (mol/m^3) - Model 1	$5.5x10^4$	Assumed
CO_2 Overall Composition - Model 2	0.005	Assumed
H_2O Overall Composition - Model 2	0.95	Assumed
MeOH Overall Composition - Model 2	0.045	Assumed
ξ_{H2O}	2.5	[1]
ξ_{MeOH}	$2.5X_{MeOH}$	[5]

Appendix B Peng Robinson Equation of State

$$P = \frac{RT}{V-b} - \frac{a}{V(V+b)+b(V-b)}$$

$$b = \sum_i z_i b_i$$

$$b_i = .077796\frac{RT_c}{P_c}$$

$$a = (bRT)\left\{\sum_i z_i \frac{a_i}{b_i RT} + \frac{1}{q_1}\left[\frac{G_0^E}{RT} + \sum_i z_i ln\left(\frac{b}{b_i}\right)\right]\right\}$$

$$a_i = \left(.457235\frac{R^2 {T_C}^2}{P_c}\right)\alpha(T)$$

$$\alpha(T) = \left[1 + k\left(1 - \sqrt{\frac{T}{T_c}}\right)\right]^2$$

$$k = .37464 + 1.54226\omega - .26992\omega^2$$

$$ln\varphi_i = \frac{b_i}{b}(Z-1) - \ln(Z-B) - \frac{1}{2\sqrt{2}}\left[\frac{a_i}{b_i RT} + \frac{ln\gamma_i}{q_1} + \frac{1}{q_1} ln\left(\frac{b}{b_i}\right) + \frac{1}{q_1} ln\left(\frac{b_i}{b} - 1\right)\right] ln\left[\frac{Z + (1+\sqrt{2})B}{Z + (1-\sqrt{2})B}\right]$$

$$B = \frac{bP}{RT}$$

$$Z^3 - (1-B)Z^2 + (A - 2B - 3B^2)Z - (AB - B^2 - B^3) = 0$$

The largest root of the above equation is the compressibility of the vapor phase and the smallest is that of the liquid phase.

$$A = \frac{aP}{R^2 T^2}$$

Works Cited

[1] S. F. Baxter, V. S. Battaglia, and R. E. White, "Methanol Fuel Cell Model: Anode," *Journal of The Electrochemical Society*, vol. 146, pp. 437-447, Feb. 1999.

[2] J.P. Meyers and J. Newman, "Simulation of the Direct Methanol Fuel Cell," *Journal of The Electrochemical Society*, vol. 149, 2002, pp. A710-A717.

[3] J.P. Meyers and J. Newman, "Simulation of the Direct Methanol Fuel Cell," *Journal of The Electrochemical Society*, vol. 149, 2002, pp. A718-A728.

[4] J.P. Meyers and J. Newman, "Simulation of the Direct Methanol Fuel Cell," *Journal of The Electrochemical Society*, vol. 149, 2002, pp. A729-A735.

[5] K. Scott, P. Argyropolous, K. Sundmacher, "A Model for the Liquid Feed Direct Methanol Fuel Cell," *Journal of Electroanalytical Chemistry*, vol. 477, pp. 97-110, 1999.

[6] J. Nordlund and G. Lindbergh, "A Model for the Porous Direct Methanol Fuel Cells Anode," *Journal of The Electrochemical Society*, vol. 149, 2002, pp. A1107-A1113.

[7] E. Birgersson, J. Nordlund, H. Ekstrom, M. Vynnycky, and G. Lindbergh, "Reduced Two-Dimensional One-Phase Model for Analysis of the Anode of a DMFC," *Journal of The Electrochemical Society,*vol. 150, 2003, pp. A1368-A1376.

[8] R. Chen and T.S. Zhao, "Mathematical Modeling of a Passive-Feed DMFC With Heat Transfer Effect,"Journal of Power Sources, vol. 152, Dec. 2005, pp. 122-130.

[9] K. Scott, P. Argyropoulos, and K. Sundmacher, "A Model for the Liquid Feed Direct Methanol Fuel Cell," *Journal of Electroanalytical Chemistry*, vol. 477, 1999, pp. 97-110.

[10] P. Argyropoulos, K. Scott, and W. M. Taama, "Carbon Dioxide Evolution Patterns in Direct Methanol Fuel Cells," *Electrochimica Acta*, vol. 44, 1999, pp. 3575-3584.

[11] E. Birgersson, J. Nordlund, M. Vynnycky, C. Picard, and G. Lindbergh, "Reduced Two-Phase Model for Analysis of the Anode of a DMFC," *Journal of The Electrochemical Society*, vol. 151, Nov. 2004, pp. A2157-A2172.

[12] P. Argyropoulos, K. Scott, and W. M. Taama, "Modelling Pressure Distribution and Anode/Cathode Streams Vapour-Liquid Equilibrium Composition in Liquid Feed Direct Methanol Fuel Cells," Chemical Engineering Journal, vol. 78, 2000, pp. 29-41.

[13] Z. H. Wang and C. Y. Wang, "Mathematical Modeling of Liquid-Feed Direct Methanol Fuel Cells,"*Journal of The Electrochemical Society*, vol. 150, 2003, pp. A508-A519.

[14] W.W. Yang and T.S. Zhao, "Two-Phase, Mass-Transport Model for Direct Methanol Fuel Cells With Effect of Non-Equilibrium Evaporation and Condensation," *Journal of Power Sources*, vol. 174, 2007 pp. 136-147.

[15] J. Ge and H. Liu, "A Three-Dimensional Two-Phase Flow Model for a Liquid-Fed

Direct Methanol Fuel Cell," *Journal of Power Sources*, vol. 163, Oct. 2006, pp. 907-915.
[16] T.Z. Yan and T. C. Jen, "Two-Phase Flow Modeling of Liquid-Feed Direct Methanol Fuel Cell," *International Journal of Heat and Mass Transfer*, vol. 51, Mar. 2007, pp. 1192-1204.
[17] T. Schultz and K. Sundmacher, "Rigorous Dynamic Model of a Direct Methanol Fuel Cell Based on Maxwell-Stefan Mass Transport Equations and a Flory-Huggins Activity Model: Formulation and Experimental Validation," *Journal of Power Sources*, vol. 145, Feb. 2005, pp. 435-463.
[18] S. Basu, C.-Y. Wang, and K. S. Chen, "Phase Change in a Polymer Electrolyte Fuel Cells," *Journal of The Electrochemical Society*, vol. 156, 2009, pp. B748-B756.
[19] G. Q. Lu and C. Y. Wang, "Electrochemical and Flow Characterization of a Direct Methanol Fuel Cell," *Journal of Power Sources*, vol. 134, Jan. 2004, pp. 33-40.
[20] B. Krishnamurthy and S. Deepalochani, "Effect of PTFE Content on the Performance of a Direct Methanol Fuel Cell," *International Journal of Hydrogen Energy*, vol. 34, Sept. 2008, pp. 446-452.
[21] J. Zhang, G.-P. Yin, Q.-Z. Lai, Z.-B. Wang, K.-D. Cai, and P. Liu, "The Influence of Anode Gas Diffusion Layer on the Performance of Low-Temperature DMFC," *Journal of Power Sources*, vol. 168, 2007, pp. 453-458.
[22] V. B. Oliveira, D. S. Falcao, C. M. Rangel, and A. M. F. R. Pinto, "A Comparative Study of Approaches to Direct Methanol Fuel Cells Modelling," *International Journal of Hydrogen Energy*, vol. 32, pp. 415-424, 2007.
[23] T.S. Zhao, C. Xu, R. Chen, and W.W. Yang, "Mass Transport Phenomena in Direct Methanol Fuel Cells," *Progress in Energy and Combustion Science*, vol. 35, Jan. 2009, pp. 275-292.
[24] S.K. Kamarudin, F. Achmad, and W.R.W. Daud, "Overview on the Application of Direct Methanol Fuel Cell (DMFC) for Portable Electronic Devices," *International Journal of Hydrogen Energy*, vol. 34, Jun. 2009, pp. 6902-6916.
[25] A. Z. Weber, R. M. Darling, and J. Newman, "Modeling Two-Phase Behavior in PEFCs," *Journal of The Electrochemical Society*, vol. 151, 2004, pp. A1715-A1727.
[26] A. Z. Weber and J. Newman, "Effects of Microporous Layers in Polymer Electrolyte Fuel Cells," *Journal of The Electrochemical Society*, vol. 152, 2005, pp. A677-A688.
[27] A. Weber and J. Newman, "Modeling Gas-Phase Flow in Porous Media," *International Communications in Heat and Mass Transfer*, vol. 32, Jul. 2005, pp. 855-960.
[28] A. Weber and J. Newman, "Modeling Gas-Phase Transport in Polymer-Electrolyte Fuel Cells," *ECS Transactions*, vol. 1, 2006, pp. 61-66.
[29] H. Orbey and S. I. Sandler, Modeling Vapor-Liquid Equilibria: Cubic Equations of State and Their Mixing Rules, Cambridge University Press, 1998.
[30] M. A. Gess, R. P. Danner, and M. Nagvekar, Thermodynamic Analysis of Vapor-Liquid Equilbria: Recommended Models and a Standard Data Base, American Institute of Chemical Engineers, 1991.
[31] S. M. Walas, Phase Equilibrium Chemical Engineering, Butterworth Publishers,

1985.
[32] K. S. Pedersen and P. L. Christensen, Phase Behavior of Petroleum Reservoir Fluids, Taylor & Francis Group, 2007.
[33] A. Firoozabadi, Thermodynamics of Hydrocarbon Reservoirs, McGraw-Hill Professional Book Group, 1998.
[34] M. L. Michelsen, "A Modified Huron-Vidal Mixing Rule for Cubic Equations of State," *Fluid Phase Equilibria*, vol. 60, pp. 213-219, 1990.
[35] D. S. Abrams and J. M. Prausnitz, "Statistical Thermodynamics of Liquid Mixtures: A New Expression for the Excess Gibbs Energy of Partially or Completely Miscible Systems," *American Institute of Chemical Engineers Journal*, vol. 21, pp. 116-128, 1975.
[36] D. Geana and R. Steiner, "Prediction of VLE and VLLE in Ternary Systems Water+Alcohol+CO_2," *Physical Chemistry*, 2001.
[37] Design Institute for Physical Properties 801 Project, 350 CB, Brigham Young University, Provo, UT 84602.
[38] A. A. Shapiro and E. H. Stenby, "Thermodynamics of the Multicomponent Vapor-Liquid Equilibrium Under Capillary Pressure Difference," *Fluid Phase Equilibria*, vol. 178, pp. 17-32, 2001.
[39] A.I. Brusilovsky, "Mathematical Simulation of Phase Behavior of Natural Multicomponent Systems at High Pressures With an Equation of State," *Society of Petroleum Engineers Reservoir Engineering*, p. 117, Feb. 1992.
[40] R. Helmig, Multiphase Flow and Transport Processes in the Subsurface, Springer-Verlag, 1997.
[41] J.S. Newman and K. E. Thomas-Alyea, Electrochemical Systems, Wiley-IEEE, 2004.
[42] K. Scott, W. Taama, and J. Cruickshank, "Performance and Modelling of a Direct Methanol Solid Polymer Electrolyte Fuel Cell," *Journal of Power Sources*, vol. 65, pp. 159-171,1997.
[43] M. J. W. Frank, J. A. M. Kuipers, and W. P. M. van Swaaij, "Diffusion Coefficients and Viscosities of CO_2 + H_2O, CO_2 + CH_3OH, NH_3 + H_2O, and NH_3 + CH_3OH Liquid Mixtures," *Journal of Chemical Engineering Data*, vol. 41, pp. 297-302, 1996.
[44] C. L. Yaws, Handbook of Transport Property Data: Viscosity, Thermal Conductivity, and Diffusion Coefficients of Liquids and Gases, Gulf Publishing Company, 1995.
[45] E. L. Cussler, Diffusion: Mass Transfer in Fluid Systems, Cambridge University Press, 1984.

Vita

Joshua Joseph Garvin was born April 2, 1986 in Riverside, California to Richard and Gail Garvin. He attended elementary school through high school in Springfield, Virginia. After graduating from high school, he attended the Massachusetts Institute of Technology (MIT) for college where he was awarded the degree of BS in Mechanical Engineering in the spring of 2008. While attending MIT, Joshua performed research under Professor Mary Boyce at the MIT Institute for Soldier Nanotechnologies where he studied the effect of the composition of PET on its mechanical response to high rates of strain. He also performed research under Professor Clark Colton on examining new methods of differentiating embryonic stem cells into other cell types. During his time at MIT he also had an externship with Aurora Flight Science designing and building an airplane wing transport structure as well as at Parsons Corporation where he modeled and computer simulated subway train fires inside tunnels. While at the University of Texas at Austin, Joshua worked in the Meyers research group performing modeling work on direct methanol fuel cells.

Permanent address: 8616 Arley Drive, Springfield, VA 22152

This thesis was typed by the author